[American Journal of Science, Vol. 314, February, 2014, P. 508–547, DOI 10.2475/02.2014.03]

GEOCHEMISTRY AND GEOCHRONOLOGY OF MESOPROTEROZOIC BASEMENT ROCKS FROM THE EASTERN AMERY ICE SHELF AND SOUTHWESTERN PRYDZ BAY, EAST ANTARCTICA: IMPLICATIONS FOR A LONG-LIVED MAGMATIC ACCRETION IN A CONTINENTAL ARC

XIAOCHUN LIU*,†, BOR-MING JAHN**, YUE ZHAO*, JIAN LIU*, and LIUDONG REN***

ABSTRACT. The high-grade metamorphic rocks from the eastern Amery Ice Shelf and southwestern Prydz Bay of East Antarctica represent reworked Rayner Complex during the late Neoproterozoic/Cambrian metamorphism. These Mesoproterozoic basement rocks can provide important information for the earlier tectonic evolution of the Rayner orogen. Chemical compositions of the mafic granulites from the Søstrene Island and Munro Kerr Mountains area suggest that their protoliths resemble Nb-enriched arc basalts, whereas those from the McKaskle-Mistichelli Hills, Reinbolt Hills and Manning Nunataks show typical characteristics of island arc basalts. Nd isotopic analyses yielded initial Nd isotope compositions, expressed as $\varepsilon_{Nd}(T)$ values, ranging from +4.1 to −0.4 for the former, and mostly from −3.2 to −4.7 for the latter. The felsic orthogneisses have the characteristics of volcanic arc granites, and one fifth of the samples belong to high Sr/Y types. The felsic orthogneisses yielded $\varepsilon_{Nd}(T)$ values of −2.4 to −7.6 and Nd depleted-mantle model ages of 2.2 to 1.9 Ga, implying an important episode of crustal formation in the Paleoproterozoic. The high Sr/Y orthogneisses have high K_2O/Na_2O ratios (>1), positive Eu anomalies, significant HREE depletion and negative $\varepsilon_{Nd}(T)$ values, suggesting their derivation from partial melting of garnet-bearing K-rich mafic sources at the lower crust of the continental arc. Geochronological data give protolith ages ranging from 1380 to 1020 Ma for these arc-related rocks, indicating a long-lived magmatic accretion in the Rayner continental arc for ~360 Ma. In addition, a younger island arc (<1080 Ma) was probably formed in the south of the Fisher oceanic arc. Coupled with the available data for the adjacent areas, we propose that the tectonic process of the Rayner orogen involved the collision of several island arcs with East Antarctica (the Lambert Terrane or the Ruker craton), followed by the closure of ocean and final collision of the Indian craton with the newly accreted Antarctic margin.

Key words: Mesoproterozoic, basement rock, magmatic accretion, continental arc, East Antarctica

INTRODUCTION

The Prince Charles Mountains-Prydz Bay region in East Antarctica provides a relatively well-exposed section (compared to much of Antarctica) of metamorphic Mesoproterozoic basement rocks, known as the Rayner Complex. This complex extends more than 1000 km from Enderby Land in the west to Princess Elizabeth Land in the east. The Rayner Complex is probably continuous with the Eastern Ghats Belt of India, forming a unified Rayner orogen through the collision of the Indian craton with East Antarctica during the late Mesoproterozoic/early Neoproterozoic (Yoshida, 1995; Mezger and Cosca, 1999; Kelly and others, 2002). However, the tectonic setting and oceanic subduction-accretion processes operating before continental collision remain little known. Previous geochemical studies indicate that the felsic orthogneisses from

* Key Laboratory of Paleomagnetism and Tectonic Reconstruction of Ministry of Land and Resources, Institute of Geomechanics, Chinese Academy of Geological Sciences, Beijing 100081, China
** Department of Geological Sciences, National Taiwan University, Taipei 10699, Taiwan
*** Institute of Geology, Chinese Academy of Geological Sciences, Beijing 100037, China
† Corresponding author: Tel: +86-10-88815038; Fax: +86-10-68422326; E-mail: liuxchqw@cags.ac.cn

the northern Prince Charles Mountains have the characteristics of I- and S-type granites (Sheraton and others, 1996; Stephenson, 2000; Mikhalsky and others, 2001). Some workers considered that their protoliths were formed in an Andean-type active continental margin (Munksgaard and others, 1992; Sheraton and others, 1996; Mikhalsky and others, 2001), but others argued that an intracontinental setting could not be ruled out (Stephenson, 2000; Wang, ms, 2002). Moreover, geochemical and isotopic data on mafic granulites suggest that the development of this active continental margin could have involved remnants of plume-related oceanic plateau and backarc basins (Mikhalsky and Sheraton, 2011). This complicates the understanding of the tectonic evolution of the Rayner orogen.

The high-grade metamorphic rocks from the eastern Amery Ice Shelf and southwestern Prydz Bay (that is, the Prydz Belt) represent reworked Rayner Complex during the late Neoproterozoic/Cambrian metamorphism and deformation. The area is dominated by felsic orthogneisses and mafic granulites. Some of these rocks, particularly those from larger outcrops, have been dated with the SHRIMP zircon U-Pb method (Liu and others, 2007a, 2009a; Wang and others, 2008; Grew and others, 2012). Four major magmatic episodes at 1380, 1210 to 1170, 1130 to 1120 and 1060 to 1020 Ma have been recognized. The three older episodes are mainly recorded in the Prydz Bay coastline and McKaskle-Mistichelli Hills, and the youngest is found in the Reinbolt Hills and Manning Nunataks. However, the limited age data available from isolated exposures are insufficient to properly characterize the time frame of magmatic episodes and the regional trends of age distribution. Thus, a comprehensive geochronological investigation is still required, which can also provide a solid base for the geochemical study.

In this contribution we present new geochemical and U-Pb zircon age data for the mafic granulites and felsic orthogneisses from the eastern Amery Ice Shelf-southwestern Prydz Bay area. We present evidence that the protoliths of the metamorphic rocks, including some mafic granulites with geochemical characteristics of Nb-enriched basalts, were formed in a continental arc setting. A long-lived magmatic accretion in the continental arc during the Mesoproterozoic may have lasted for ~360 Ma. Coupled with the available data from adjacent areas, a new tectonic model will be presented to illustrate our view of tectonic processes, involving arc-continent collision followed by continent-continent collision between the Indian craton and East Antarctica (the Lambert Terrane or the Ruker craton) during the early Neoproterozoic.

GEOLOGICAL SETTING

The Prince Charles Mountains-Prydz Bay region is located in Kemp, MacRobertson and Princess Elizabeth Lands of East Antarctica. The region comprises four Archean/Paleoproterozoic cratonic blocks, a late Mesoproterozoic Fisher Terrane, an early Neoproterozoic Rayner Complex and a late Neoproterozoic/Cambrian Prydz Belt (fig. 1). Four Archaean/Paleoproterozoic blocks include the Ruker Terrane in the southern Prince Charles Mountains, the Lambert Terrane in the northern Mawson Escarpment, the Vestfold Block and the Rauer Group in Prydz Bay. Each preserves distinct crustal histories and therefore do not form remnants of a single unified craton (Harley, 2003; Boger, 2011). The Fisher Terrane crops out in the southern sector of the northern Prince Charles Mountains, where mafic-felsic volcanism and intrusion occurred at 1300 to 1020 Ma, followed by amphibolite facies metamorphism at 1020 to 940 Ma (Beliatsky and others, 1994; Kinny and others, 1997; Mikhalsky and others, 1999, 2001). All these igneous rocks have calc-alkaline affinities and Nd model ages (T_{DM}) of 1.8 to 1.6 Ga (Mikhalsky and others, 1996, 2006). The Rayner Complex is mainly exposed in the northern Prince Charles Mountains and adjacent Mawson Coast. It is characterized by regional granulite facies metamorphism accompanied by widespread charnockitic and granitic magmatism at 1000 to 900 Ma (Kinny and others,

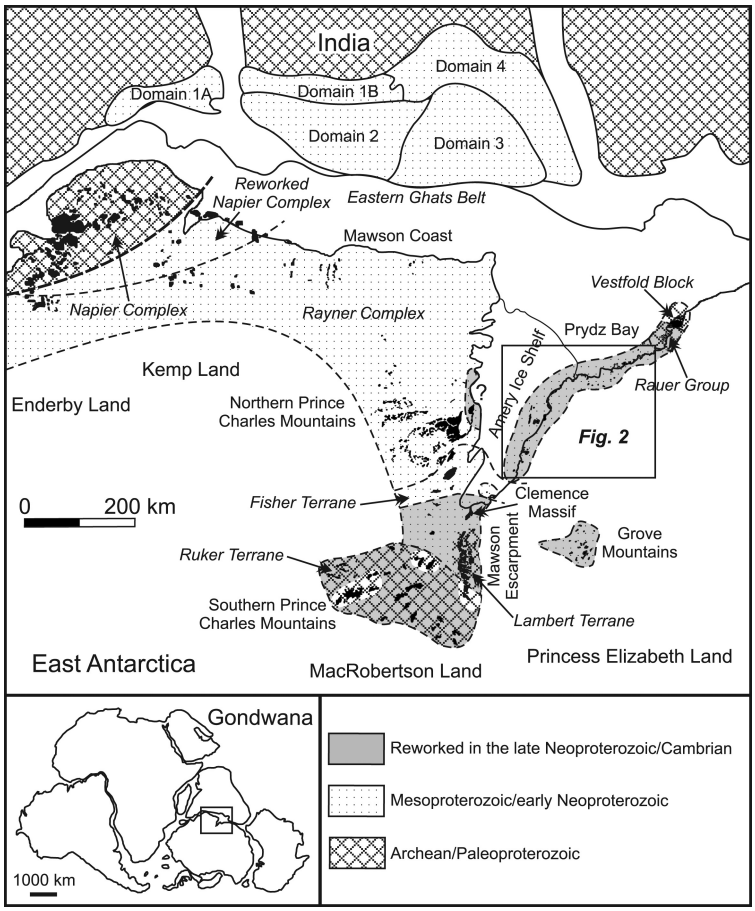

Fig. 1. Geological sketch map of the Prince Charles Mountains-Prydz Bay region and its relation to the Eastern Ghats Belt of India (modified after Mikhalsky and others, 2001; Rickers and others, 2001; Fitzsimons, 2003; Dasgupta and others, 2013). Inset shows its location in Gondwana at ~500 Ma. Domains 1A, 1B, 2, 3 and 4 of the Eastern Ghats Belt were divided based on isotopic (Nd model age) characters (Rickers and others, 2001).

1997; Boger and others, 2000; Carson and others, 2000; Halpin and others, 2007, 2012). The protolith ages of mafic granulites and felsic orthogneisses dominating the Rayner Complex are not well-constrained. Their T_{DM} ages range from 2.2 to 1.6 Ga (Young and others, 1997; Zhao and others, 1997a).

The Prydz Belt is exposed in Prydz Bay, eastern Amery Ice Shelf and the Grove Mountains. The high-grade metamorphic rocks in Prydz Bay and eastern Amery Ice Shelf comprise two lithological associations: mafic-felsic composite orthogneisses and migmatitic paragneisses, which are attributed to the basement and cover sequences, respectively (Fitzsimons and Harley, 1991; Carson and others, 1995; Fitzsimons, 1997). Geochronological studies suggest that the basement orthogneisses were originally emplaced during the period 1380 to 1020 Ma, with T_{DM} ages of 2.4 to 1.7 Ga (Sheraton and others, 1984; Zhao and others, 1995, 2003; Liu and others, 2007a, 2009a; Wang and others, 2008; Grew and others, 2012), while the cover sequences might have been deposited during the late Mesoproterozoic (Dirks and Wilson, 1995; Wang and others, 2008; Grew and others, 2012) or Neoproterozoic (Hensen and Zhou, 1995; Zhao and

others, 1995; Kelsey and others, 2008). The major tectonothermal events, including deformation, high-grade metamorphism and emplacement of syn- to post-orogenic granites, took place between 550 and 490 Ma (Zhao and others, 1992, 1995, 1997b; Hensen and Zhou, 1995; Carson and others, 1996; Fitzsimons and others, 1997; Grew and others, 2013a). However, a widespread metamorphic event accompanied by the charnockite intrusion at 990 to 900 Ma was also recognized (Hensen and Zhou, 1995; Wang and others, 2008; Liu and others, 2009a; Grew and others, 2012). In contrast, the rocks from the Grove Mountains yielded young protolith ages of 920 to 910 Ma, with two T_{DM} age groups of 1.8 to 1.6 and 2.5 to 2.3 Ga (Liu and others, 2007b). These rocks experienced only a single metamorphic cycle at 570 to 500 Ma (Liu and others, 2006, 2007b, 2009b).

SAMPLES AND ANALYTICAL TECHNIQUES

Sample Description

Twenty-five mafic granulite and 35 felsic orthogneiss samples from the Søstrene Island, Munro Kerr Mountains area (including the Hamm Peak, Svarthausen Nunatak and Meknattane Nunataks), McKaskle-Mistichelli Hills, Reinbolt Hills and Manning Nunataks in the eastern Amery Ice Shelf-southwestern Prydz Bay area were chosen for major and trace element analyses. Of them 30 samples were also analyzed for Nd isotopic compositions. In addition, 4 felsic orthogneisses from the above outcrops and 2 others from the Statler Hills and Jennings Promontory were selected for sensitive high-resolution ion microprobe (SHRIMP) U-Pb zircon analyses. The sample localities are shown in figure 2. The mineral assemblages of the samples are presented in table 1.

Mafic granulites occur as continuous layers or lenses within felsic orthogneisses. The granulite layers are typically a few meters to several tens of meters wide. Rarely, a layer may reach 2 km wide as that occurring in the Reinbolt Hills. Most granulite samples exhibit an equilibrium paragenesis of clinopyroxene + orthopyroxene + hornblende + plagioclase + opaque, with or without minor biotite and/or quartz. However, sample 23-23 has no plagioclase, whereas sample 149-3 contains olivine and spinel. Samples 23-10 to 23-34 were taken from a large mafic granulite body about 100×300 m^2 in size from Søstrene Island, and 24-2 and 24-6 were collected from a folded dike-like layer from the same outcrop. Some of these samples contain garnet porphyroblasts, which exhibit two-stage retrograde decompression (Thost and others, 1991). Another garnet-bearing sample 80-1 was taken from a folded mafic granulite layer 1.5 m wide in the McKaskle Hills. This thin layer might be a deformed dike intruded in felsic orthogneisses.

Felsic orthogneisses are the dominant rock type of the eastern Amery Ice Shelf-southwestern Prydz Bay area. They show weak, moderate to strong foliations and, in many cases, are interleaved with mafic granulites. All primary magmatic minerals and fabrics have been obliterated by the granulite facies metamorphism. Thus, it is difficult to determine whether these felsic orthogneisses are metamorphosed intrusive or extrusive rocks (Sheraton and others, 1996). Most samples consist of orthopyroxene, biotite, plagioclase, K-feldspar, quartz and opaque, with or without garnet. The intermediate type commonly contains minor clinopyroxene and hornblende. Some samples, particularly those from the Munro Kerr Mountains area, do not contain orthopyroxene. Their mineral assemblage is garnet + biotite + plagioclase + K-feldspar + quartz + opaque. Samples 41-1 and 41-4 are dike rocks from the Hamm Peak, whereas sample 117-2 was collected from a small enclave about 45×80 cm^2 in the Jennings Promontory charnockite.

Analytical Techniques

Whole-rock chemical analyses were carried out at the National Research Center for Geoanalysis, Chinese Academy of Geological Sciences. Major element abundances,

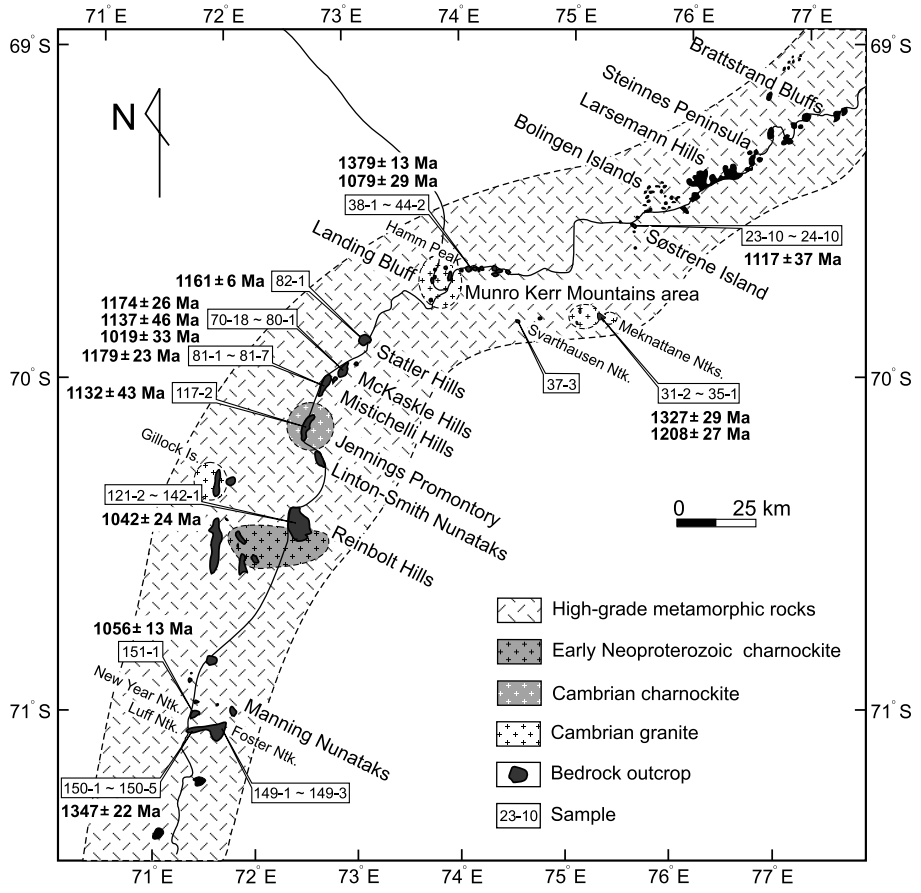

Fig. 2. Geological sketch map of the eastern Amery Ice Shelf and southwestern Prydz Bay (modified after Mikhalsky and others, 2001; Liu and others, 2009a). The localities of the studied samples and their protolith ages obtained with SHRIMP U-Pb zircon dating (Liu and others, 2007a, 2009a; this paper) are indicated.

except FeO and LOI, which were determined by a wet chemical method, were measured by XRF (3080E) after fusion of sample powder with lithium tetraborate. Relative standard deviations are better than 5 percent. Trace element concentrations were measured by inductively coupled plasma-mass spectrometry (ICP-MS) (TJA PQ ExCell), following the method of Wang and others (2003). Sample powders were digested with HF + HNO_3 mixture in high-pressure Teflon bombs on a hot-plate for 24 h. After complete digestion, sample solution was evaporated to incipient dryness, refluxed with 6N HNO_3, and heated again to incipient dryness to remove organic matter. The sample was then dissolved in 2 ml of 3N HNO_3 and diluted with Milli-Q water (18 MX) to a final dilution factor of 2000. The detection limit for trace elements is about 0.1 ppm. Analytical uncertainties are less than 5 percent for trace elements with concentrations $\geq$20 ppm and 5 to 10 percent for concentrations $\leq$20 ppm. The analytical results are presented in tables 2 and 3. The chondritic values used in construction of REE patterns and the primitive mantle (PM) values used in spidergrams are from Sun and McDonough (1989).

Nd isotopic analyses were performed at the Institute of Geology and Geophysics, Chinese Academy of Sciences. The analytical procedures are the same as reported by

TABLE 1

Locations, mineral assemblages and protolith ages of the studied samples

Location	Sample	Mineral assemblage
Mafic granulite		
Søstrene Island	23-10	Grt + Cpx + Opx + Hbl + Pl + Oq
	23-13	Cpx + Opx + Hbl + Pl + Oq
	23-16	Grt + Cpx + Opx + Hbl + Pl + Oq
	23-17	Cpx + Opx + Hbl + Pl + Oq
	23-23	Cpx + Opx + Hbl + Oq
	23-34	Grt + Cpx + Opx + Hbl + Pl + Oq
	24-2	Grt + Cpx + Opx + Hbl + Pl + Oq
	24-6	Cpx + Opx + Hbl + Oq
Munro Kerr Mountains area	33-10	Cpx + Opx + Pl + Oq
	38-6	Cpx + Opx + Hbl + Pl + Oq
	41-16	Cpx + Opx + Hbl + Bt + Pl
McKaskle-Mistichelli Hills	71-5	Cpx + Opx + Hbl + Bt + Pl + Oq
	72-1	Cpx + Opx + Hbl + Pl
	74-1	Cpx + Opx + Hbl + Bt + Pl + Oq
	78-1	Cpx + Opx + Hbl + Bt + Pl + Oq
	79-5	Cpx + Opx + Bt + Pl
	80-1	Grt + Cpx + Opx + Hbl + Pl + Oq
Reinbolt Hills	121-2	Cpx + Opx + Bt + Pl + Qtz + Oq
	134-1	Opx + Pl + Qtz + Oq
	138-1	Cpx + Opx + Hbl + Bt + Pl + Qtz + Oq
	142-1	Cpx + Opx + Hbl + Bt + Pl + Qtz + Oq
Manning Nunataks	149-1	Cpx + Opx + Hbl + Bt + Pl + Oq
	149-3	Ol + Cpx + Hbl + Pl + Spl
	150-4	Cpx + Opx + Hbl + Bt + Pl + Qtz + Oq
	150-5	Cpx + Opx + Hbl + Bt + Pl + Oq
Felsic orthogneiss		
Søstrene Island	23-28	Grt + Opx + Bt + Pl + Kfs + Qtz + Oq
	24-10	Grt + Opx + Bt + Pl + Kfs + Qtz + Oq
Munro Kerr Mountains area	31-2	Grt + Opx + Bt + Pl + Kfs + Qtz + Oq
	32-1	Cpx + Opx + Hbl + Bt + Pl + Kfs + Qtz + Oq
	35-1	Grt + Opx + Bt + Pl + Kfs + Qtz + Oq
	37-3	Grt + Opx + Bt + Pl + Kfs + Qtz + Oq
	38-1	Grt + Opx + Bt + Pl + Kfs + Qtz + Oq
	38-7	Grt + Bt + Pl + Kfs + Qtz + Oq
	43-8	Grt + Bt + Pl + Kfs + Qtz + Oq
	44-2	Grt + Bt + Pl + Kfs + Qtz + Oq
	41-1	Grt + Pl + Kfs + Qtz + Oq
	41-4	Grt + Bt + Pl + Kfs + Qtz + Oq
McKaskle-Mistichelli Hills	70-18	Opx + Bt + Pl + Kfs + Qtz + Oq
	72-5	Opx + Bt + Pl + Kfs + Qtz + Oq
	72-7	Grt + Opx + Bt + Pl + Kfs + Qtz + Oq
	73-1	Cpx + Opx + Hbl + Bt + Pl + Kfs + Qtz + Oq
	74-8	Opx + Bt + Pl + Kfs + Qtz + Rt + Oq
	74-10	Opx + Bt + Pl + Kfs + Qtz + Oq
	79-1	Opx + Bt + Pl + Kfs + Qtz + Rt + Oq
	79-2	Opx + Bt + Pl + Kfs + Qtz + Oq
	79-3	Opx + Bt + Pl + Kfs + Qtz + Oq
	81-1	Cpx + Opx + Hbl + Pl + Kfs + Qtz + Oq
	81-7	Opx + Hbl + Bt + Pl + Kfs + Qtz + Oq_
Statler Hills	82-1	Opx + Hbl + Bt + Pl + Kfs + Qtz + Oq
Jennings Promontory	117-2	Opx + Hbl + Pl + Kfs + Qtz + Oq
Reinbolt Hills	126-1	Cpx + Opx + Hbl + Bt + Pl + Qtz + Oq
	126-2	Cpx + Opx + Hbl + Bt + Pl + Qtz + Oq
	127-1	Grt + Opx + Bt + Pl + Kfs + Qtz + Oq
	129-1	Grt + Opx + Bt + Pl + Kfs + Qtz + Oq
	131-1	Grt + Opx + Bt + Pl + Kfs + Qtz + Oq
	135-1	Bt + Pl + Kfs + Qtz + Oq
	136-1	Opx + Pl + Kfs + Qtz + Oq
	139-1	Opx + Bt + Pl + Kfs + Qtz + Oq
	140-1	Opx + Bt + Pl + Kfs + Qtz
	141-1	Opx + Pl + Kfs + Qtz + Oq
Manning Nunataks	150-1	Opx + Pl + Kfs + Qtz + Oq
	151-1	Opx + Bt + Pl + Kfs + Qtz + Oq

Abbreviations: Bt = biotite; Cpx = clinopyroxene; Grt = garnet; Hbl = hornblende; Kfs = K-feldspar; Ol = olivine;Opx = orthopyroxene; Oq = opaque; Pl = plagioclase; Qtz = quartz; Rt = rutile; Spl = spinel.

TABLE 2

Chemical compositions of mafic granulites

Locality	Søstrene Island								Munro Kerr Mountains area			McKaskle-Mistichelli Hills		
Sample	23-10	23-13	23-16	23-17	23-23	23-34	24-2	24-6	33-10	38-6	41-16	71-5	72-1	74-1
SiO_2 (wt%)	43.72	46.77	47.80	47.40	47.99	44.94	42.67	47.49	43.30	43.34	47.72	47.03	47.46	47.31
TiO_2	2.40	2.31	2.10	1.60	1.52	2.09	3.41	1.61	3.33	3.68	0.59	1.13	0.53	0.41
Al_2O_3	11.46	10.84	12.34	10.16	8.31	13.09	13.56	9.80	12.76	12.07	15.03	13.98	15.78	17.04
Fe_2O_3	2.83	1.96	1.90	1.89	1.97	1.94	5.86	2.31	0.75	6.45	1.34	4.41	2.09	2.40
FeO	11.69	11.44	11.62	10.74	10.54	12.43	12.52	10.15	19.24	14.66	9.09	8.87	6.94	5.87
MnO	0.28	0.20	0.20	0.20	0.18	0.26	0.26	0.18	0.28	0.31	0.17	0.18	0.15	0.16
MgO	11.90	13.04	9.99	13.43	18.18	10.33	8.01	15.59	6.34	5.84	12.41	10.40	10.44	10.31
CaO	12.68	11.28	10.56	11.96	9.01	12.31	11.08	10.29	10.94	10.74	10.08	10.30	13.57	13.46
Na_2O	1.16	1.08	1.60	1.45	1.22	0.92	1.49	1.28	0.36	1.69	1.16	2.10	1.30	1.41
K_2O	0.14	0.07	0.06	0.11	0.19	0.09	0.16	0.36	0.59	0.28	1.23	1.07	0.54	0.64
P_2O_5	0.28	0.29	0.62	0.32	0.17	0.34	0.27	0.16	0.05	0.10	0.06	0.09	0.08	0.11
LOI	0.93	0.90	0.90	0.93	1.02	0.87	0.89	0.84	1.51	0.51	0.66	0.63	0.65	0.88
Total	99.47	100.18	99.69	100.19	100.30	99.61	100.18	100.06	99.45	99.67	99.54	100.19	99.53	100.00
Mg#	62	66	60	68	75	59	47	72	39	36	70	62	70	72
Rb (ppm)	2.75	1.07	0.67	1.70	1.64	2.51	2.23	7.27	81.6	1.77	129	13.0	5.95	9.33
Sr	131	279	349	173	109	186	221	139	194	118	89.3	143	362	297
Ba	9.72	5.51	6.96	8.47	6.41	12.4	22.2	39.6	85.5	39.5	51.1	42.8	32.3	67.7
Pb	0.66	0.31	0.74	0.50	0.32	0.44	1.13	0.99	4.91	4.01	3.46	6.73	5.21	5.87
Th	0.39	0.07	0.02	0.021	0.043	0.08	0.12	0.23	0.58	0.04	0.70	0.61	1.45	0.96
U	0.12	0.01	0.02	0.01	0.02	0.03	0.04	0.07	0.26	0.02	0.45	0.08	0.25	0.36
Zr	57.8	54.1	32.5	48.0	55.7	61.6	75.8	59.2	30.8	32.5	29.8	51.4	32.3	32.8
Hf	1.57	1.63	1.31	1.40	1.70	1.85	2.15	1.61	0.88	1.05	0.67	1.3	0.85	0.87
Nb	11.2	8.78	9.70	5.51	7.08	11.3	18.9	8.14	3.54	4.86	2.24	3.34	2.87	2.68
Ta	0.73	0.61	1.05	0.38	0.47	0.82	1.16	0.57	0.25	0.37	0.18	0.26	0.24	0.31
Sc	57.9	47.3	46.0	38.9	31.6	41.5	49.1	34.9	81.0	95.0	33.0	61.8	54.8	43.0
V	503	410	390	334	301	396	525	355	1876	1064	215	410	257	171
Cr	501	835	665	1116	1410	612	50.0	1206	6.17	5.07	149	200	380	469
Co	62.3	70.2	50.8	68.1	80.6	57.2	60.4	72.1	80.2	66.1	65.7	57.2	48.5	54.1
Ni	158	305	110	359	787	135	106	544	57.0	12.4	325	123	125	219
Cu	67.7	41.8	44.2	22.1	51.1	62.0	36.8	95.9	147	37.8	6.03	34.3	7.11	99.7
Zn	101	131	133	117	120	115	162	119	216	172	106	118	64.8	64.9
Ga	17.4	18.5	19.9	16.3	15.3	19.5	23.0	17.1	24.3	24.2	14.8	17.8	14.9	13.7
Y	34.0	20.4	26.6	20.9	19.7	32.2	33.7	22.7	23.8	29.6	13.9	26.0	10.6	10.5
K/Rb	423	543	743	537	962	298	596	411	60	1313	79	683	753	569
Rb/Sr	0.021	0.004	0.002	0.010	0.015	0.013	0.010	0.052	0.421	0.015	1.445	0.091	0.016	0.031
K/Ba	120	105	72	108	246	60	60	75	57	59	200	208	139	78
Rb/Ba	0.28	0.19	0.10	0.20	0.26	0.20	0.10	0.18	0.95	0.05	2.52	0.30	0.18	0.14
Th/U	3.25	11.00	1.00	1.50	1.87	2.50	3.33	3.48	2.23	2.00	1.56	7.35	5.80	2.67
La	5.70	3.85	4.70	5.06	7.92	6.84	10.1	9.21	5.85	5.42	2.90	5.44	11.8	7.01
Ce	19.0	14.6	15.8	17.9	24.5	21.2	29.6	25.8	14.9	15.1	7.83	13.9	26.5	16.7
Pr	2.76	2.29	2.43	2.57	3.16	2.95	4.46	3.34	1.86	2.03	0.99	1.78	2.83	1.99
Nd	13.6	12.0	12.7	12.6	14.2	14.7	22.7	15.6	8.44	9.97	4.81	8.42	11.1	8.20
Sm	4.27	3.86	4.09	3.80	3.76	4.57	6.77	4.4	2.85	3.34	1.49	2.88	2.42	2.07
Eu	1.55	1.31	1.42	1.36	1.36	1.60	2.17	1.43	1.02	1.42	0.67	1.08	0.68	0.7
Gd	6.57	5.23	5.88	5.22	5.41	6.77	8.66	6.06	4.24	5.13	2.31	4.37	3.09	2.75
Tb	1.14	0.78	0.94	0.80	0.75	1.05	1.23	0.85	0.69	0.87	0.40	0.72	0.38	0.35
Dy	7.14	4.63	5.73	4.76	4.44	6.71	7.20	4.92	4.61	5.78	2.59	4.85	2.21	2.04
Ho	1.39	0.87	1.13	0.90	0.86	1.37	1.42	0.94	0.96	1.23	0.55	1.03	0.42	0.41
Er	3.65	2.14	2.92	2.32	2.16	3.57	3.61	2.44	2.71	3.38	1.57	2.95	1.15	1.14
Tm	0.48	0.27	0.41	0.30	0.27	0.46	0.46	0.31	0.36	0.48	0.22	0.41	0.16	0.16
Yb	3.06	1.76	2.62	1.92	1.68	2.83	2.81	1.90	2.38	3.15	1.55	2.64	1.12	1.06
Lu	0.44	0.26	0.38	0.27	0.25	0.40	0.41	0.27	0.36	0.50	0.24	0.41	0.18	0.15
REE	70.8	53.9	61.2	59.8	70.7	75.0	102	77.5	51.2	57.8	28.1	50.9	64.0	44.7
$(La/Yb)_N$	1.34	1.57	1.29	1.89	3.38	1.73	2.58	3.48	1.76	1.23	1.34	1.48	7.56	4.74
Eu/Eu*	0.89	0.89	0.88	0.93	0.92	0.88	0.87	0.85	0.90	1.05	1.10	0.93	0.76	0.90

TABLE 2
(continued)

Locality	McKaskle-Mistichelli Hills			Reinbolt Hills				Manning Nunataks			
Sample	78-1	79-5	80-1	121-2	134-1	138-1	142-1	149-1	149-3	150-4	150-5
SiO_2 (wt%)	49.40	48.66	44.15	51.77	52.22	52.25	52.62	44.50	42.26	48.15	45.78
TiO_2	0.41	0.85	1.58	2.10	2.10	1.92	1.35	3.10	1.10	0.91	2.57
Al_2O_3	7.12	13.41	13.05	14.98	15.53	16.34	16.36	12.41	13.52	15.41	17.72
Fe_2O_3	1.36	1.73	2.72	2.42	1.68	2.44	2.39	2.78	2.55	1.70	1.95
FeO	8.08	8.84	15.07	10.47	11.05	8.50	7.35	15.61	5.28	11.08	13.09
MnO	0.17	0.19	0.32	0.20	0.21	0.18	0.15	0.29	0.13	0.24	0.24
MgO	16.88	11.24	8.73	5.53	5.35	4.58	5.46	6.32	8.94	8.05	4.87
CaO	12.57	9.99	11.71	7.95	8.52	7.22	8.57	10.88	22.46	10.94	8.60
Na_2O	0.46	1.46	0.74	2.22	0.97	2.93	2.97	1.54	0.19	1.13	2.36
K_2O	1.76	2.26	0.59	1.15	1.30	0.97	1.58	0.76	0.28	1.42	1.10
P_2O_5	0.16	0.25	0.15	0.72	0.71	0.68	0.43	0.32	1.79	0.07	0.44
LOI	1.11	0.98	0.90	0.67	0.39	1.68	1.10	0.91	0.94	0.88	1.14
Total	99.48	99.86	99.71	100.18	100.03	99.69	100.33	99.42	99.44	99.98	99.86
Mg#	78	68	50	46	46	46	53	41	70	56	39
Rb (ppm)	114	174	32.9	45.0	26.7	12.6	55.5	14.6	5.44	46.2	28.5
Sr	29.8	249	42.7	400	411	369	515	140	458	197	209
Ba	123	296	75.4	1313	1231	464	1057	95.1	207	169	228
Pb	2.85	7.76	3.92	16.5	9.84	9.83	14.0	3.90	6.92	7.61	6.50
Th	5.13	4.22	2.65	3.37	0.90	0.67	0.84	0.86	43.6	0.99	2.42
U	1.54	0.57	0.55	0.73	0.31	0.12	0.35	0.33	8.05	0.14	0.24
Zr	37.7	36.0	65.9	399	309	157	281	146	147	60.0	145
Hf	1.03	1.23	1.83	9.12	6.79	3.73	6.34	4.37	3.06	1.78	3.82
Nb	3.16	7.62	9.47	22.8	28.2	26.6	14.5	9.74	11.8	3.87	27.6
Ta	0.27	0.53	0.51	1.11	1.04	1.02	0.52	0.61	0.90	0.21	1.36
Sc	69.0	44.6	63.9	29.6	27.2	20.5	26.1	61.9	36.3	38.2	48.9
V	250	275	491	268	262	249	219	549	201	280	348
Cr	1594	968	82.8	52.8	103	103	72.1	68.1	147	169	117
Co	73.9	49.1	66.4	49.2	39.3	32.6	37.5	53.4	24.1	58.6	45.6
Ni	337	228	90.7	52.6	49.8	42.0	53.3	27.7	20.8	53.7	42.6
Cu	43.6	20.4	60.0	55.1	29.3	76.0	28.0	70.6	8.80	11.8	67.6
Zn	65.1	124	211	152	152	136	111	175	72.8	144	116
Ga	9.11	16.2	22.1	23.4	23.3	21.3	21.0	25.6	19.7	20.2	26.9
Y	11.7	28.2	40.6	57.7	59.5	37.0	40.4	70.9	63.4	30.0	75.8
K/Rb	128	108	149	212	404	639	236	432	427	255	320
Rb/Sr	3.826	0.699	0.770	0.113	0.065	0.034	0.108	0.104	0.012	0.235	0.136
K/Ba	119	63	65	7	9	17	12	66	11	70	40
Rb/Ba	0.93	0.59	0.44	0.03	0.02	0.03	0.05	0.15	0.03	0.27	0.13
Th/U	3.33	7.40	4.82	4.62	2.90	5.58	2.40	2.61	5.42	7.07	10.08
La	8.14	28.7	33.2	71.3	55.5	32.0	49.5	18.0	107.0	14.1	30.4
Ce	19.2	70.9	99.5	157	140	87.0	108	47.2	207.0	35.4	76.3
Pr	2.40	8.08	11.0	18.0	17.0	10.8	12.3	6.56	21.0	4.61	9.24
Nd	11.0	31.3	39.4	70.3	71.5	48.2	48.3	30.3	71.6	19.9	40.4
Sm	2.83	6.70	7.79	13.5	14.7	10.4	9.34	9.23	12.5	5.23	9.83
Eu	0.71	1.91	1.77	3.09	3.14	2.42	2.31	2.83	2.48	1.43	2.56
Gd	3.33	8.29	10.2	11.6	13.0	8.58	8.07	10.8	10.2	5.17	10.8
Tb	0.43	1.04	1.30	1.83	2.00	1.27	1.26	2.00	1.79	0.92	1.91
Dy	2.40	5.56	7.67	10.1	10.8	6.65	7.01	12.1	9.88	5.36	12.0
Ho	0.47	1.13	1.65	1.98	2.14	1.28	1.36	2.54	2.08	1.09	2.50
Er	1.31	3.08	4.58	5.66	5.85	3.47	3.81	7.16	6.08	3.06	7.12
Tm	0.17	0.42	0.64	0.80	0.76	0.47	0.52	1.06	0.90	0.42	1.01
Yb	1.09	2.84	4.22	4.98	4.97	2.95	3.21	6.85	5.71	2.85	6.37
Lu	0.16	0.43	0.66	0.72	0.71	0.42	0.48	0.98	0.83	0.40	0.91
REE	53.6	170	224	371	342	216	255	158	459	99.9	211
$(La/Yb)_N$	5.36	7.25	5.64	10.27	8.01	7.78	11.06	1.88	13.44	3.55	3.42
Eu/Eu*	0.71	0.78	0.61	0.74	0.68	0.76	0.79	0.86	0.65	0.83	0.76

TABLE 3

Chemical compositions of felsic orthogneisses

Locality	Søstrene Island				Munro Kerr Mountains area							
Sample	23-28	24-10	31-2	32-1	35-1	37-3	38-1	38-7	43-8	44-2	41-1	41-4
SiO_2 (wt%)	70.98	66.91	67.78	65.02	67.91	70.41	64.67	72.91	68.50	74.77	73.25	72.61
TiO_2	0.60	0.92	0.76	0.58	0.80	0.70	0.66	0.43	0.84	0.27	0.08	0.15
Al_2O_3	13.21	13.95	13.62	14.83	13.56	13.59	15.17	12.21	12.68	12.50	14.44	14.30
Fe_2O_3	0.51	1.07	1.17	1.10	0.39	1.10	0.73	0.35	0.29	0.14	0.14	0.32
FeO	3.43	4.28	6.13	5.23	6.54	3.61	4.99	5.46	6.65	1.74	1.86	1.74
MnO	0.05	0.05	0.13	0.11	0.15	0.08	0.06	0.13	0.11	0.03	0.06	0.05
MgO	0.73	1.16	2.31	2.83	1.44	1.00	2.32	1.66	2.72	1.01	0.62	0.67
CaO	2.41	3.31	2.54	5.89	3.39	3.88	3.31	2.80	1.45	1.70	2.84	1.77
Na_2O	2.24	2.23	2.79	2.62	2.46	2.39	2.56	1.70	1.76	2.27	3.11	2.20
K_2O	5.38	4.92	2.20	0.71	1.73	2.50	4.40	1.45	3.97	5.17	2.52	5.67
P_2O_5	0.54	0.43	0.04	0.09	0.21	0.17	0.10	0.03	0.04	0.10	0.04	0.07
LOI	0.40	0.67	0.70	1.08	0.92	0.45	0.69	0.36	0.42	0.39	0.40	0.41
Total	100.48	99.90	100.17	100.09	99.50	99.88	99.66	99.49	99.43	100.09	99.36	99.96
K_2O/Na_2O	2.40	2.21	0.79	0.27	0.70	1.05	1.72	0.85	0.81	2.58	2.26	2.28
ASI	0.95	0.93	1.18	0.94	1.12	0.99	1.01	1.29	1.29	1.01	1.11	1.10
Rb (ppm)	246	165	95.3	44.8	64.1	102	175	60.0	220	249	59.4	270
Sr	134	177	173	200	205	224	460	151	197	306	412	376
Ba	887	1401	446	370	1020	1513	1548	332	1115	1466	1014	2073
Pb	26.0	18.4	18.7	13.9	18.0	17.6	34.2	18.0	30.6	53.6	32.2	56.8
Th	6.37	8.74	9.69	9.82	29.3	5.81	12.0	26.8	26.5	36.4	16.6	58.1
U	0.47	0.30	0.95	0.69	1.56	0.48	0.68	1.09	0.87	1.49	0.57	2.00
Zr	466	433	263	132	442	396	194	252	293	160	115	234
Hf	9.26	7.69	5.59	3.03	8.77	7.59	4.14	5.43	6.32	3.92	2.93	4.92
Nb	17.3	20.0	9.86	12.2	16.1	11.9	10.5	7.68	11.6	6.99	1.70	2.85
Ta	0.95	0.83	0.52	0.69	0.99	0.60	0.55	0.36	0.43	0.19	0.09	0.14
Sc	9.49	12.6	24.3	22.9	23.4	15.9	16.9	21.1	22.6	5.70	7.96	8.73
V	27.5	63.9	141	146	51.7	55.7	105	53.2	126	17.1	6.20	19.3
Cr	8.70	16.8	89.1	50.8	21.0	18.4	83.3	29.5	90.0	8.20	3.57	14.9
Co	4.51	8.29	18.1	20.6	9.92	9.07	8.74	12.5	15.1	3.59	2.60	3.50
Ni	5.01	6.88	31.5	22.7	7.32	12.2	6.23	18.4	20.2	6.21	3.98	5.27
Cu	7.34	14.3	56.3	17.9	9.81	20.3	25.1	19.6	19.8	10.7	4.45	8.53
Zn	63.0	78.9	98.6	74.8	71.8	71.2	94.5	46.2	78.1	29.8	14.9	20.7
Ga	20.4	21.3	18.9	17.4	18.9	18.0	21.3	16.0	18.2	18.4	15.9	19.4
Y	29.1	25.3	39.4	34.4	62.0	31.6	10.8	56.9	48.1	14.9	21.6	25.3
K/Rb	182	248	192	132	224	203	209	201	150	172	352	174
Rb/Sr	1.84	0.93	0.55	0.22	0.31	0.46	0.38	0.40	1.12	0.81	0.14	0.72
K/Ba	50	29	41	16	14	14	24	36	30	29	21	23
Rb/Ba	0.28	0.12	0.21	0.12	0.06	0.07	0.11	0.18	0.20	0.17	0.06	0.13
Th/U	13.55	29.13	10.20	14.23	18.8	12.10	17.65	24.59	30.46	24.43	29.12	29.05
$10^4Ga/Al$	2.92	2.89	2.62	2.22	2.63	2.50	2.65	2.48	2.71	2.78	2.08	2.56
Sr/Y	4.60	7.00	4.39	5.81	3.31	7.09	42.59	2.65	4.10	20.54	19.07	14.86
La	69.3	68.6	38.3	25.4	71.9	55.8	55.5	55.4	68.6	67.7	32.5	107
Ce	130	123	69.9	51.6	140	103	91.9	110	129	134	61.5	211
Pr	12.6	13.6	6.61	5.44	13.2	9.75	8.21	10.6	12.4	13.5	6.05	19.5
Nd	45.3	51.7	23.4	21.3	48.3	36.5	27.3	37.6	44.0	47.3	21.3	68.7
Sm	8.50	9.35	5.17	5.53	9.16	6.36	4.24	8.41	8.96	9.07	3.96	12.9
Eu	2.19	3.14	1.82	1.24	2.80	3.38	3.09	1.30	2.36	2.48	1.64	3.10
Gd	11.6	12.1	8.10	7.86	14.5	8.98	6.08	12.9	13.2	10.6	5.28	15.6
Tb	1.35	1.18	1.12	1.09	2.10	1.02	0.51	1.82	1.58	0.86	0.60	1.28
Dy	6.80	5.67	7.25	6.55	12.9	5.88	2.27	11.3	9.3	3.38	3.66	5.22
Ho	1.24	1.10	1.60	1.30	2.53	1.25	0.46	2.33	1.99	0.62	0.88	1.00
Er	3.16	2.86	4.78	3.60	6.50	3.80	1.39	6.52	5.74	1.73	2.99	3.09
Tm	0.38	0.34	0.68	0.49	0.84	0.56	0.19	0.93	0.81	0.22	0.46	0.41
Yb	2.26	2.12	4.80	3.29	5.26	4.13	1.39	6.17	5.40	1.45	3.34	2.85
Lu	0.32	0.31	0.73	0.48	0.78	0.67	0.22	0.94	0.84	0.20	0.53	0.39
REE	295	295	174	135	331	241	203	266	304	293	145	452
$(La/Yb)_N$	22.00	23.21	5.72	5.54	9.80	9.69	28.64	6.44	9.11	33.49	6.98	26.93
Lu	0.32	0.31	0.73	0.48	0.78	0.67	0.22	0.94	0.84	0.20	0.53	0.67

TABLE 3
(continued)

Locality	McKaskle-Mistichelli Hills										
Sample	70-18	72-5	72-7	73-1	74-8	74-10	79-1	79-2	79-3	81-1	81-7
SiO_2 (wt%)	68.99	65.72	73.10	63.26	65.94	69.65	66.56	64.05	62.34	61.04	69.76
TiO_2	0.52	0.69	0.33	0.84	0.51	0.62	0.51	0.60	0.68	0.70	0.52
Al_2O_3	13.75	14.46	13.65	15.03	13.10	14.02	12.93	13.46	13.81	14.12	14.00
Fe_2O_3	2.31	3.17	1.09	2.49	0.59	2.27	0.63	1.20	0.82	1.54	0.82
FeO	3.20	4.02	1.38	4.47	5.17	2.84	5.08	5.42	6.61	7.06	3.25
MnO	0.10	0.14	0.03	0.11	0.10	0.08	0.10	0.12	0.13	0.17	0.07
MgO	1.65	2.60	0.73	2.30	5.67	1.64	5.59	6.23	6.93	3.61	1.71
CaO	4.09	5.48	3.54	5.69	3.68	4.21	4.23	4.21	4.34	7.18	3.75
Na_2O	2.60	2.27	2.11	2.49	1.92	2.22	2.21	1.86	1.98	2.37	2.06
K_2O	2.01	0.97	3.22	2.22	2.45	2.53	1.05	1.54	1.54	1.14	3.92
P_2O_5	0.12	0.13	0.07	0.22	0.11	0.14	0.08	0.11	0.12	0.13	0.10
LOI	0.43	0.49	0.43	0.50	0.47	0.36	0.46	0.61	0.53	0.47	0.46
Total	99.77	100.14	99.68	99.62	99.71	100.58	99.43	99.41	99.83	99.53	100.42
K_2O/Na_2O	0.77	0.43	1.53	0.89	1.28	1.14	0.48	0.83	0.78	0.48	1.90
ASI	0.99	0.98	1.02	0.89	1.05	1.00	1.04	1.09	1.08	0.78	0.97
Rb (ppm)	84.6	36.3	124	117	148	108	56.2	123	113	35.9	175
Sr	219	336	417	396	158	343	151	157	144	267	300
Ba	449	422	1650	831	462	987	178	271	275	344	1180
Pb	16.7	10.6	20.1	17.3	12.9	17.5	11.2	9.49	9.70	8.97	14.4
Th	1.94	0.63	0.77	3.98	2.18	0.94	8.70	3.19	0.71	1.76	0.71
U	0.19	0.21	0.20	0.34	0.23	0.23	0.23	0.23	0.14	0.22	0.20
Zr	164	146	176	301	135	213	97.9	86.5	69.5	111	143
Hf	3.53	3.08	3.74	5.62	3.08	4.66	2.50	2.24	1.75	2.88	3.13
Nb	8.81	8.40	4.21	14.1	6.81	8.06	6.47	8.92	8.19	7.72	5.94
Ta	0.40	0.38	0.19	0.79	0.39	0.50	0.32	0.61	0.39	0.57	0.35
Sc	29.9	34.8	8.94	35.6	18.9	20.6	17.9	18.8	25.1	34.8	10.5
V	104	175	43.9	172	89.7	88.9	92.8	114	122	217	88.1
Cr	28.4	63.0	18.6	37.5	568	29.5	547	575	629	98.0	40.9
Co	13.3	20.4	4.92	19.0	27.8	11.9	26.9	31.6	33.9	27.9	13.1
Ni	10.5	16.0	8.04	17.2	115	12.8	103	114	116	23.7	13.4
Cu	14.6	40.4	6.00	67.1	9.12	13.1	10.7	10.6	11.8	26.6	14.2
Zn	76.3	100	25.2	103	77.8	65.7	81.2	93.3	93.0	116	57.7
Ga	20.2	20.8	16.5	22.6	16.8	16.3	17.3	18.8	18.7	18.6	14.9
Y	21.8	19.4	9.89	53.3	11.6	23.8	10.1	13.1	16.1	36.7	9.20
K/Rb	197	222	216	158	137	194	155	104	113	264	186
Rb/Sr	0.39	0.11	0.30	0.30	0.94	0.32	0.37	0.78	0.79	0.13	0.58
K/Ba	37	19	16	22	44	21	49	47	46	28	28
Rb/Ba	0.19	0.09	0.08	0.14	0.32	0.11	0.32	0.45	0.41	0.10	0.15
Th/U	10.21	3.00	3.85	11.71	9.48	4.09	37.83	13.87	5.07	8.00	3.55
10^4Ga/Al	2.78	2.72	2.28	2.84	2.42	2.20	2.53	2.64	2.56	2.49	2.01
Sr/Y	10.05	17.32	42.16	7.43	13.62	14.41	14.95	11.99	8.94	7.28	32.61
La	39.7	39.2	31.6	50.0	24.2	30.6	31.5	24.3	22.5	19.7	15.3
Ce	71.1	72.4	47.6	108	46.7	60.7	58.4	47.2	43.6	48.8	27.3
Pr	7.45	6.89	4.93	12.0	4.94	6.90	5.98	5.07	4.74	6.28	3.01
Nd	27.1	25.0	16.9	49.0	18.0	26.9	20.5	18.6	17.4	26.8	11.3
Sm	5.46	4.70	3.11	11.7	3.15	5.31	3.19	3.33	3.38	6.60	2.24
Eu	1.59	1.74	2.48	2.75	1.00	1.23	0.92	0.88	0.87	1.35	1.06
Gd	7.76	6.49	4.82	15.3	2.63	4.99	2.39	2.84	3.08	6.33	2.10
Tb	0.88	0.70	0.49	1.94	0.38	0.74	0.34	0.41	0.47	1.01	0.28
Dy	4.77	3.80	2.43	10.9	2.13	4.47	1.90	2.36	2.86	6.35	1.61
Ho	0.91	0.79	0.41	2.20	0.41	0.88	0.38	0.46	0.57	1.30	0.31
Er	2.38	2.29	1.05	6.01	1.20	2.38	1.08	1.26	1.65	3.74	0.90
Tm	0.30	0.34	0.13	0.79	0.16	0.31	0.16	0.17	0.23	0.52	0.13
Yb	1.88	2.37	0.79	5.09	1.04	1.86	0.95	1.14	1.52	3.25	0.85
Lu	0.28	0.38	0.11	0.75	0.17	0.28	0.15	0.17	0.24	0.51	0.12
REE	172	167	117	276	106	148	128	108	103	133	66.5
$(La/Yb)_N$	15.15	11.86	28.69	7.05	16.69	11.80	23.78	15.29	10.62	4.35	12.91
Lu	0.75	0.96	1.95	0.63	1.03	0.72	0.98	0.85	0.81	0.63	1.47

TABLE 3
(continued)

Locality	Reinbolt Hills										Manning Ntks.	
Sample	126-1	126-2	127-1	129-1	131-1	135-1	136-1	139-1	140-1	141-1	150-1	151-1
SiO_2 (wt%)	60.78	56.03	67.32	71.95	66.98	74.67	74.52	57.31	73.66	74.88	75.06	69.31
TiO_2	1.03	1.25	0.53	0.24	0.47	0.15	0.08	1.56	0.16	0.22	0.32	0.68
Al_2O_3	15.81	17.58	14.96	14.27	16.14	13.51	13.59	16.60	11.73	12.73	11.96	13.98
Fe_2O_3	2.29	1.71	0.63	0.55	0.42	0.49	0.49	0.74	1.07	0.59	1.22	0.44
FeO	5.26	6.23	4.35	1.19	2.34	0.63	0.52	7.83	1.28	1.24	1.17	3.36
MnO	0.13	0.13	0.14	0.02	0.05	0.01	0.02	0.15	0.02	0.03	0.02	0.05
MgO	3.24	3.77	2.06	0.77	1.03	0.53	0.61	3.75	1.73	0.55	0.15	0.76
CaO	6.22	7.03	4.02	2.00	2.79	2.34	2.23	6.41	0.63	2.20	1.16	2.39
Na_2O	2.81	3.40	3.74	2.56	3.17	2.71	2.47	2.82	1.70	2.19	2.44	2.48
K_2O	1.21	1.31	0.96	5.65	5.29	4.03	4.76	1.24	6.63	4.62	5.64	5.60
P_2O_5	0.40	0.45	0.11	0.12	0.42	0.03	0.05	0.53	0.02	0.03	0.04	0.23
LOI	1.07	1.19	0.67	0.48	0.39	0.27	1.04	0.96	0.88	0.55	0.43	0.38
Total	100.25	100.08	99.49	99.80	99.49	99.37	100.38	99.90	99.51	99.83	99.61	99.66
K_2O/Na_2O	0.43	0.39	0.26	2.21	1.67	1.49	1.93	0.44	3.90	2.11	2.31	2.26
ASI	0.92	0.89	1.03	1.02	1.01	1.03	1.02	0.94	1.06	1.01	0.98	0.97
Rb (ppm)	16.8	19.4	13.4	216	126	115	101	41.2	244	176	174	166
Sr	353	449	147	220	240	165	216	307	117	197	42.1	115
Ba	554	590	172	1611	2633	1295	2026	401	1712	2003	876	767
Pb	12.1	13.4	20.5	32.9	37.7	21.6	34.7	11.2	32.4	21.0	11.8	31.8
Th	0.62	1.11	1.02	1.02	16.5	1.70	0.44	0.65	15.7	1.02	2.41	12.9
U	0.27	0.69	1.11	0.33	1.32	0.31	0.24	0.30	0.72	0.43	0.65	0.66
Zr	209	827	208	137	159	123	87.1	408	151	172	340	450
Hf	4.74	20.1	5.14	3.68	4.24	3.62	2.45	8.78	5.15	4.45	9.37	12.1
Nb	14.4	16.3	17.5	5.87	9.63	4.61	1.16	21.0	8.49	4.25	10.9	23.1
Ta	0.59	0.63	1.01	0.20	0.45	0.18	0.05	0.78	0.21	0.26	0.38	0.63
Sc	16.1	15.4	13.6	3.65	6.74	1.76	1.36	27.6	8.36	5.66	4.62	10.0
V	158	205	89.4	30.1	43.7	21.0	13.6	195	18.1	30.8	12.3	29.7
Cr	47.1	59.2	40.0	17.2	17.3	9.08	8.24	80.6	2.37	7.60	4.25	7.70
Co	21.4	23.5	14.3	4.92	6.93	3.11	2.47	24.8	3.42	4.62	2.15	6.05
Ni	26.6	34.6	29.6	10.4	11.8	7.32	4.53	29.5	3.70	4.82	2.62	7.25
Cu	32.7	33.8	37.7	20.8	14.1	10.1	5.35	38.4	3.65	5.54	12.1	10.8
Zn	87.7	86.8	82.0	34.0	42.1	18.6	17.1	110	59.5	29.8	18.0	61.8
Ga	19.9	22.6	19.0	15.1	16.0	13.2	12.3	22.2	14.2	15.2	18.1	21.0
Y	29.0	29.9	32.9	5.47	17.2	1.33	3.91	28.4	18.8	4.01	19.7	28.5
K/Rb	598	561	595	217	349	291	391	250	226	218	268	280
Rb/Sr	0.05	0.04	0.09	0.98	0.53	0.70	0.47	0.13	2.09	0.89	4.13	1.44
K/Ba	18	18	46	29	17	26	20	26	32	19	53	61
Rb/Ba	0.03	0.03	0.08	0.13	0.05	0.09	0.05	0.10	0.14	0.09	0.20	0.22
Th/U	2.30	01.61	0.92	3.09	12.50	5.48	1.83	2.17	21.81	2.37	3.71	19.55
$10^4Ga/Al$	2.38	2.43	2.40	2.00	1.87	1.85	1.71	2.53	2.29	2.26	2.86	2.84
Sr/Y	12.17	15.02	4.47	40.22	13.95	124.06	55.24	10.81	6.22	49.13	2.14	4.04
La	38.6	42.8	23.7	20.3	35.8	18.5	8.28	40.1	37.8	17.9	48.2	54.5
Ce	84.6	90.1	42.2	27.4	77.7	26.4	10.8	84.2	69.6	20.4	41.5	96.6
Pr	10.1	10.3	4.66	2.77	10.2	2.95	1.37	9.27	7.00	2.18	8.10	12.0
Nd	40.4	39.6	16.6	9.07	39.7	9.35	4.65	39.5	25.7	6.39	28.3	45.1
Sm	7.77	7.45	3.38	1.58	7.76	1.17	0.98	8.60	4.83	1.00	4.54	8.71
Eu	2.10	2.03	0.93	1.08	1.89	0.89	0.99	1.61	0.91	1.64	0.94	1.79
Gd	6.37	6.14	3.29	1.52	5.21	0.78	1.37	7.17	4.22	0.96	3.93	6.91
Tb	0.98	0.95	0.69	0.21	0.63	0.08	0.13	1.06	0.60	0.11	0.64	1.04
Dy	5.22	4.96	4.85	0.89	3.01	0.25	0.73	5.23	3.26	0.56	3.75	5.21
Ho	0.98	0.98	1.04	0.17	0.57	0.04	0.14	0.98	0.65	0.12	0.78	1.06
Er	2.73	2.82	2.80	0.41	1.67	0.13	0.37	2.58	2.00	0.38	2.38	2.83
Tm	0.36	0.40	0.35	0.05	0.29	0.02	0.06	0.34	0.33	0.06	0.34	0.38
Yb	2.28	2.42	2.10	0.33	2.13	0.15	0.41	2.26	2.29	0.47	2.41	2.55
Lu	0.33	0.39	0.32	0.06	0.34	0.03	0.07	0.31	0.39	0.08	0.37	0.39
REE	203	211	107	65.8	187	60.7	30.4	203	160	52.3	146	239
$(La/Yb)_N$	12.14	12.69	8.10	44.12	12.06	88.47	14.49	12.73	11.84	27.32	14.35	15.33
Lu	0.89	0.89	0.84	2.10	0.86	2.68	2.61	0.61	0.60	5.05	0.66	0.68

TABLE 4

Sm-Nd isotopic analyses for mafic granulites and felsic orthogneissess

Sample	Age (ref.)	Sm (ppm)	Nd (ppm)	$^{147}Sm/^{144}Nd$	$^{143}Nd/^{144}Nd$	$\pm 2\sigma$	$f_{Sm/Nd}$	$\varepsilon_{Nd}(0)$	$\varepsilon_{Nd}(T)$	T_{DM} (Ga)
Mafic granulite										
23-17	1150 Ma	3.541	12.35	0.1733	0.512561	0.000011	-0.12	-1.5	1.9	2.21
23-34	1150 Ma	4.331	14.88	0.1760	0.512462	0.000012	-0.11	-3.4	-0.4	2.77
24-2	1150 Ma	6.718	24.13	0.1683	0.512439	0.000011	-0.14	-3.9	0.3	2.38
24-6	1150 Ma	4.069	15.41	0.1597	0.512400	0.000011	-0.19	-4.6	0.8	2.11
38-6	1200 Ma	3.065	9.736	0.1903	0.512629	0.000012	-0.03	-0.2	0.8	3.37
41-16	1200 Ma	1.305	4.382	0.1800	0.512715	0.000011	-0.08	1.5	4.1	1.96
71-5	1150 Ma	2.608	8.407	0.1875	0.512743	0.000017	-0.04	2.1	3.4	2.36
72-1	1150 Ma	2.159	10.19	0.1282	0.511881	0.000011	-0.34	-14.8	-4.7	2.25
78-1	1150 Ma	2.559	10.60	0.1460	0.512042	0.000011	-0.26	-11.6	-4.2	2.48
134-1	1050 Ma	13.71	69.23	0.1197	0.511946	0.000014	-0.39	-13.5	-3.2	1.95
142-1	1050 Ma	8.543	46.30	0.1115	0.511873	0.000015	-0.43	-14.9	-3.5	1.90
149-1	1050 Ma	7.913	27.26	0.1755	0.512525	0.000012	-0.11	-2.2	0.6	2.48
150-4	1050 Ma	5.118	19.74	0.1533	0.512279	0.000014	-0.22	-7.0	-1.2	2.19
Felsic orthogneiss										
24-10	1150 Ma	9.320	55.41	0.1017	0.511534	0.000013	-0.48	-21.5	-7.6	2.19
32-1	1200 Ma	5.173	20.97	0.1492	0.512045	0.000012	-0.24	-11.6	-4.3	2.60
35-1	1200 Ma	8.440	46.28	0.1103	0.511706	0.000014	-0.44	-18.2	-5.0	2.12
37-3	1200 Ma	5.938	35.39	0.1014	0.511671	0.000010	-0.48	-18.9	-4.3	2.00
38-1	1350 Ma	3.916	26.30	0.0900	0.511485	0.000011	-0.54	-22.5	-4.1	2.04
38-7	1200 Ma	7.999	38.36	0.1261	0.511765	0.000013	-0.36	-17.0	-6.2	2.40
44-2	1200 Ma	7.110	39.56	0.1087	0.511608	0.000011	-0.45	-20.1	-6.6	2.23
41-1	1050 Ma	4.017	22.99	0.1056	0.511624	0.000011	-0.46	-19.8	-7.6	2.14
70-18	1150 Ma	4.117	21.77	0.1144	0.511774	0.000011	-0.42	-16.9	-4.8	2.10
72-7	1150 Ma	2.479	14.12	0.1061	0.511675	0.000011	-0.46	-18.8	-5.5	2.08
74-8	1150 Ma	3.227	18.52	0.1053	0.511599	0.000011	-0.46	-20.3	-6.9	2.17
81-7	1150 Ma	2.211	11.75	0.1137	0.511759	0.000020	-0.42	-17.2	-5.0	2.11
127-1	1050 Ma	3.381	17.80	0.1171	0.511933	0.000015	-0.40	-13.8	-3.1	1.91
136-1	1050 Ma	0.931	4.836	0.1164	0.511965	0.000019	-0.41	-13.1	-2.4	1.85
139-1	1050 Ma	7.647	38.81	0.1193	0.511889	0.000013	-0.39	-14.6	-4.2	2.03
150-1	1350 Ma	3.956	25.62	0.0935	0.511411	0.000010	-0.52	-23.9	-7.6	2.20
151-1	1050 Ma	7.982	44.22	0.1091	0.511815	0.000012	-0.45	-16.1	-4.3	1.94

Liu and others (2006). Powdered samples were spiked with ^{149}Sm and ^{150}Nd and dissolved in acid ($HF + HNO_3$). Dissolution was done in Teflon bombs at about 100 °C for 10 days. Sm and Nd were separated with the conventional ion exchange techniques. Nd isotope ratios were measured with a Finnigan MAT 262 multi-collector mass spectrometer. Total procedural blanks were <100 pg for Sm and Nd. Nd isotopic fractionations were corrected against $^{146}Nd/^{144}Nd = 0.7219$. Within-run precision ($2\sigma_m$) for Nd was estimated to be ± 0.000015. During the period of data acquisition, the measured isotope ratio for Jndi-1 Nd standard was $^{143}Nd/^{144}Nd = 0.512124 \pm 0.000012$ ($2\sigma_m$). The USGS standard BCR-2, prepared with the same procedures as the samples, yielded Sm = 6.67, Nd = 29.20, $^{147}Sm/^{144}Nd = 0.1382$, and $^{143}Nd/^{144}Nd = 0.512645 \pm 0.000012$ (2σ). The analytical results are shown in table 4. Nd depleted-mantle model ages (T_{DM}) were calculated assuming a linear isotopic evolution of the depleted mantle reservoir from $\varepsilon_{Nd}(T) = 0$ at 4.56 Ga to +10 at the present.

U-Th-Pb zircon analyses were performed using the SHRIMP II ion microprobe at the Beijing SHRIMP Centre, Chinese Academy of Geological Sciences. Zircon was extracted with conventional techniques, including crushing, sieving, heavy liquid and hand picking. Zircon grains were mounted in an epoxy disc along with the TEMORA

zircon standard and polished to expose their centre. Internal structures of zircon grains were revealed by cathodoluminescence (CL) imaging. Instrumental conditions and data acquisition procedures were similar to those described by Williams (1998). A primary ion beam of 4.5 nA, 10 kV O_2^- and ~30 μm spot was used. The measured $^{206}Pb/^{238}U$ ratios were corrected with reference zircon TEMORA (416.75 ± 0.24 Ma; Black and others, 2003). Correction for common Pb was made with the measured ^{204}Pb. Ages were calculated using the programs SQUID 1.03 and ISOPLOT 3.23. The age uncertainties for individual analyses represent one standard deviation (1σ), but the calculated weighted mean $^{206}Pb/^{238}U$ or $^{207}Pb/^{206}Pb$ ages are quoted at the 95 percent confidence level. The analytical data are listed in table 5.

RESULTS

Major and Trace Elements

Mafic granulites.—Mafic granulites show a range of SiO_2 contents from 42 to 53 weight percent and a large variation of total alkalis ($Na_2O + K_2O$) from 0.5 to 4.6 weight percent. Most samples are classified as basalts to picrobasalts in the total alkali versus silica (TAS) classification by Middlemost (1994), but those from the Reinbolt Hills are basaltic andesites (fig. 3A). According to the Nb/Y versus Zr/Ti discrimination diagram of Winchester and Floyd (1977), most of them belong to subalkaline basalts and andesites/basalts, whereas those from the Reinbolt Hills mainly fall in the andesite and dacite fields (fig. 3B). In the Alkali-FeO*-MgO (AFM) diagram (Irvine and Baragar, 1971), all samples display a tholeiitic trend, except for sample 142-1 from the Reinbolt Hills, which has a calc-alkaline trend (fig. 3C). The Mg# values of the rocks are highly variable, ranging from 39 to 78, suggesting their derivation from different evolved mafic magmas.

The chondrite-normalized rare earth element (REE) patterns and primitive mantle (PM) normalized spidergrams of mafic granulites are shown in figures 4A–4J. The REE patterns of samples from Søstrene Island (named Group I mafic granulites) are weakly fractionated, with $(La/Yb)_N$ between 1.29 and 3.48 (fig. 4A). They have total REE contents of 54 to 102 ppm and negligible Eu anomalies (Eu/Eu* = 0.85-0.93). In the spidergrams (fig. 4F), the most distinguishing feature is the enrichment of Nb and Ta relative to K and La (Nb = 5.51-18.9 ppm, Nb/La = 0.88-2.28). The overall trace element abundances resemble enriched mid-ocean ridge basalts (E-MORB) except the more pronounced depletion in large ion lithophile elements (LILE) such as Rb, Ba and K, as well as high-field strength elements (HFSE) such as Th and Zr.

Samples from the Munro Kerr Mountains area (Group II mafic granulites) have nearly flat REE Patterns [$(La/Yb)_N$ = 1.23-1.76] (fig. 4B), with total REE contents of 28 to 58 ppm and almost no Eu anomalies (Eu/Eu* = 0.90-1.10). In the spidergrams (fig. 4G), no noticeable Nb and Ta anomalies relative to La were observed, but two samples (33-10 and 41-16) are considerably enriched in K and Rb. The overall patterns are also comparable with those of E-MORB.

Samples from the McKaskle-Mistichelli Hills, Reinbolt Hills and Manning Nunataks (Group III mafic granulites) displays slightly or moderately LREE-enriched patterns [$(La/Yb)_N$ = 1.48-13.44] (figs. 4C-4E), with total REE contents of 45 to 459 ppm and weakly negative Eu anomalies (Eu/Eu* = 0.61-0.93). Their trace element abundances are characterized by variable enrichment of LILE and significant depletion in Nb-Ta, Zr (Hf) and Ti (figs. 4H-4J). Sr abundances also show negative anomalies for most samples.

Felsic orthogneisses.—The SiO_2 contents of felsic orthogneisses range from 56 to 75 weight percent, $Na_2O + K_2O$ from 3.2 to 8.5 weight percent, and K_2O/Na_2O ratios vary from 0.26 to 3.90. They cover the andesite-dacite-rhyolite field in the TAS and Nb/Y-Zr/Ti classification diagrams (see figs. 3A and 3B). All samples plot in the

TABLE 5

SHRIMP U-Pb zircon analyses for felsic orthogneisses

Spot	U (ppm)	Th (ppm)	Th/U	Pb* (ppm)	Common ^{206}Pb(%)	Isotopic Ratios						Ages			
						$^{207}Pb/^{206}Pb$	±σ (%)	$^{207}Pb/^{235}U$	±σ (%)	$^{206}Pb/^{238}U$	±σ (%)	$^{207}Pb/^{206}Pb$	±σ	$^{206}Pb/^{238}U$	±σ
Sample 24-10 (Søstrene Island)															
Oscillatory-zoned core															
1.1	124	117	0.97	14.0	0.49	0.0661	3.8	1.194	4.0	0.1309	1.0	810	80	793	7
2.1	377	243	0.67	55.1	0.22	0.0722	1.6	1.689	2.3	0.1698	1.6	991	33	1011	15
3.1	282	135	0.50	40.3	0.32	0.0707	2.0	1.612	2.2	0.1655	0.8	948	41	987	7
4.1	241	155	0.66	32.1	0.66	0.0746	2.4	1.582	2.6	0.1538	1.0	1057	48	922	9
5.1	191	160	0.86	32.4	0.30	0.0776	2.7	2.102	2.8	0.1964	0.7	1138	54	1156	7
5.2	214	177	0.85	35.7	0.58	0.0745	2.7	1.983	2.8	0.1930	0.8	1056	54	1138	8
6.1	131	99	0.78	13.7	0.58	0.0637	3.8	1.066	3.9	0.1213	0.9	732	80	738	7
7.1	896	349	0.40	128.0	0.10	0.0711	2.4	1.629	2.5	0.1662	0.4	959	50	991	3
8.1	162	198	1.26	23.1	0.36	0.0701	2.1	1.596	2.2	0.1650	0.7	932	42	985	7
9.1	357	365	1.06	60.4	0.21	0.0792	1.4	2.147	1.5	0.1967	0.5	1177	28	1157	5
9.2	571	97	0.18	80.6	0.21	0.0762	1.4	1.722	1.7	0.1640	1.0	1099	28	979	9
10.1	307	170	0.57	39.9	0.14	0.0706	1.2	1.470	1.3	0.1510	0.6	945	25	907	5
11.1	177	143	0.84	19.7	0.49	0.0712	3.6	1.268	3.7	0.1291	0.8	964	74	783	6
12.1	221	134	0.63	18.5	0.39	0.0568	3.7	0.760	3.8	0.0970	0.8	483	83	597	4
13.1	462	240	0.54	57.8	0.26	0.0674	1.5	1.352	1.6	0.1454	0.6	852	31	875	5
14.1	463	223	0.50	69.4	0.22	0.0743	1.5	1.784	1.6	0.1742	0.6	1050	30	1035	6
15.1	211	211	1.03	34.2	0.21	0.0732	3.1	1.900	3.2	0.1882	0.7	1021	62	1111	7
16.1	480	262	0.56	79.5	0.18	0.0792	2.4	2.098	2.5	0.1922	0.5	1176	48	1134	5
17.1	357	285	0.83	58.1	0.07	0.0731	1.2	1.912	1.3	0.1896	0.6	1018	24	1119	6
18.1	461	273	0.61	71.6	0.13	0.0758	1.1	1.886	1.2	0.1805	0.5	1089	22	1070	5
19.1	126	631	5.19	21.5	0.49	0.0741	2.6	2.022	2.8	0.1980	0.9	1043	53	1165	9
20.1	236	131	0.57	38.9	0.22	0.0747	1.8	1.970	1.9	0.1913	0.6	1061	36	1128	7
21.1	460	136	0.31	76.5	0.11	0.0760	1.1	2.024	3.1	0.1933	2.9	1094	22	1139	30
22.1	324	134	0.43	55.9	0.10	0.0787	2.7	2.177	2.8	0.2005	0.8	1165	53	1178	8
23.1	443	117	0.27	72.7	0.08	0.0810	1.6	2.131	1.7	0.1909	0.6	1221	32	1126	6
24.1	303	133	0.45	48.1	0.14	0.0754	1.5	1.922	1.7	0.1848	0.8	1081	30	1093	8
Bright homogeneous and planar-zoned rim															
19.2	107	73	0.71	18.3	0.95	0.0698	4.1	1.895	4.2	0.1969	1.0	922	84	1159	10
25.1	436	145	0.34	68.0	0.18	0.0834	2.2	2.082	2.3	0.1810	0.7	1279	43	1073	7
26.1	57	197	3.60	7.7	0.97	0.0818	6.4	1.763	6.7	0.1564	1.8	1240	126	936	15
27.1	46	167	3.74	6.1	1.22	0.0827	8.0	1.726	8.2	0.1514	2.0	1261	156	909	17

Table 5
(continued)

Spot	U (ppm)	Th (ppm)	Th/U	Pb* (ppm)	Common ^{206}Pb(%)	Isotopic Ratios						Ages			
						$^{207}Pb/^{206}Pb$	±σ (%)	$^{207}Pb/^{235}U$	±σ (%)	$^{206}Pb/^{238}U$	±σ (%)	$^{207}Pb/^{206}Pb$	±σ	$^{206}Pb/^{238}U$	±σ
Sample 24-10 (Søstrene Island)															
Bright homogeneous and planar-zoned rim															
28.1	88	274	3.22	11.2	0.54	0.0759	3.4	1.545	3.6	0.1476	1.4	1093	67	887	11
29.1	99	126	1.31	12.6	1.23	0.0688	5.1	1.380	5.2	0.1455	1.1	892	105	876	9
30.1	57	309	5.57	7.5	0.27	0.0731	2.7	1.532	3.0	0.1520	1.3	1016	55	912	11
31.1	86	239	2.86	13.1	1.01	0.0787	5.3	1.893	5.4	0.1745	1.1	1164	104	1037	10
32.1	103	246	2.47	16.3	0.33	0.0734	2.1	1.851	2.3	0.1828	0.8	1026	42	1082	8
33.1	135	228	1.75	13.7	0.12	0.0676	1.7	1.099	1.9	0.1179	0.7	856	36	719	5
34.1	64	344	5.58	9.9	0.18	0.0749	2.0	1.872	2.2	0.1812	0.9	1067	40	1074	9
35.1	150	194	1.34	22.2	0.39	0.0709	2.1	1.676	2.1	0.1715	0.6	954	42	1020	6
36.1	89	240	2.80	14.4	0.66	0.0725	2.4	1.877	2.5	0.1878	0.8	1000	49	1109	8
37.1	103	236	2.36	13.8	0.95	0.0694	4.7	1.478	4.8	0.1544	0.8	911	97	926	7
38.1	49	293	6.12	8.3	2.33	0.0798	8.7	2.096	8.8	0.1905	1.1	1192	173	1124	12
Sample 31-2 (Meknattane Nunataks)															
Oscillatory-zoned core															
1.1	254	178	0.72	44.7	0.17	0.0843	1.1	2.370	1.2	0.2040	0.6	1299	20	1197	6
2.1	908	317	0.36	139.0	0.28	0.0798	0.9	1.955	1.0	0.1777	0.4	1193	19	1054	4
3.1	236	198	0.87	47.6	0.02	0.0863	0.8	2.793	1.0	0.2346	0.7	1346	15	1358	8
4.1	505	189	0.39	159.2	0.09	0.1210	0.6	6.117	0.7	0.3665	0.5	1971	10	2013	8
5.1	656	546	0.86	123.0	0.02	0.0834	0.5	2.506	0.6	0.2180	0.4	1278	10	1271	5
6.1	189	69	0.37	35.7	0.21	0.0835	1.3	2.523	1.5	0.2191	0.7	1281	25	1277	8
7.1	96	59	0.63	17.8	0.24	0.0874	1.9	2.581	2.2	0.2141	1.0	1370	37	1251	11
8.1	262	261	1.03	57.7	0.11	0.0878	0.9	3.098	1.1	0.2559	0.6	1378	18	1469	8
9.1	211	101	0.49	40.4	0.15	0.0839	1.3	2.569	1.5	0.2221	0.7	1290	25	1293	8
10.1	667	599	0.93	114.8	0.17	0.0815	0.9	2.248	1.0	0.1999	0.5	1235	18	1175	5
11.1	325	110	0.35	75.0	0.14	0.0977	1.0	3.618	2.1	0.2686	1.8	1580	18	1534	25
12.1	172	131	0.79	34.1	0.00	0.0851	1.3	2.706	1.6	0.2307	0.8	1317	25	1338	10
13.1	316	146	0.48	58.2	0.12	0.0840	2.5	2.484	2.5	0.2144	0.6	1293	48	1252	7
14.1	479	363	0.78	95.8	0.04	0.0858	0.8	2.751	1.0	0.2327	0.5	1333	16	1349	6
15.1	403	190	0.49	67.4	0.11	0.0847	0.9	2.271	1.1	0.1945	0.6	1309	18	1146	6
16.1	188	59	0.33	28.2	0.30	0.0812	2.3	1.952	2.7	0.1743	1.4	1226	46	1036	13
17.1	730	2500	3.54	138.2	0.24	0.0808	1.0	2.450	1.1	0.2199	0.4	1216	20	1281	5
18.1	356	230	0.67	62.8	0.19	0.0828	2.8	2.341	2.9	0.2050	0.6	1265	56	1202	6

TABLE 5
(continued)

Spot	U (ppm)	Th (ppm)	Th/U	Pb* (ppm)	Common ^{206}Pb(%)	Isotopic Ratios						Ages			
						^{207}Pb/^{206}Pb	±σ (%)	^{207}Pb/^{235}U	±σ (%)	^{206}Pb/^{238}U	±σ (%)	^{207}Pb/^{206}Pb	±σ	^{206}Pb/^{238}U	±σ
Sample 31-2 (Meknattane Nunataks															
Dark planar- and sector-zoned mantle															
8.2	980	8	0.01	113.7	0.10	0.0710	3.7	1.320	3.7	0.1349	0.4	956	76	816	3
11.2	1499	11	0.01	183.1	0.06	0.0706	1.6	1.382	1.6	0.1421	0.3	945	32	856	3
18.2	903	16	0.02	111.3	0.02	0.0876	4.4	1.733	4.4	0.1434	0.4	1374	85	864	3
19.1	1407	12	0.01	174.5	0.01	0.0731	0.6	1.454	0.7	0.1443	0.3	1016	12	869	3
20.1	974	27	0.03	109.8	0.01	0.0677	0.8	1.225	1.0	0.1311	0.6	861	16	794	4
21.1	751	14	0.02	84.7	0.08	0.0708	2.8	1.281	3.0	0.1312	1.1	953	56	794	8
22.1	1166	15	0.01	149.0	0.07	0.0715	2.3	1.465	2.3	0.1487	0.4	970	47	894	3
23.1	852	39	0.05	79.8	0.03	0.0630	10.5	0.946	10.5	0.1090	0.4	707	223	667	3
24.1	858	28	0.03	104.3	0.10	0.0736	11.6	1.433	11.6	0.1413	0.7	1030	234	852	6
25.1	1483	52	0.04	199.2	0.13	0.0869	0.9	1.871	1.0	0.1562	0.3	1357	18	936	3
26.1	468	25	0.05	57.5	0.08	0.0674	1.3	1.328	1.4	0.1430	0.5	849	27	861	4
27.1	975	25	0.03	106.5	0.08	0.0677	2.1	1.185	2.7	0.1270	1.8	859	43	771	13
28.1	434	27	0.06	54.5	0.13	0.0675	1.2	1.358	1.3	0.1459	0.5	853	25	878	5
29.1	591	76	0.13	70.8	0.18	0.0722	1.3	1.387	1.4	0.1393	0.5	991	27	841	4
30.1	836	13	0.02	91.1	0.08	0.0694	2.4	1.213	2.4	0.1267	0.5	912	48	769	3
Sample 41-1 (Hamm Peak)															
Oscillatory-zoned core															
1.1	106	59	0.58	16.2	0.22	0.0751	2.0	1.842	2.2	0.1780	1.0	1070	39	1056	10
2.1	325	232	0.74	50.8	0.09	0.0755	1.0	1.896	1.1	0.1822	0.5	1082	20	1079	5
3.1	202	91	0.47	30.5	0.68	0.1020	1.5	2.462	1.7	0.1751	0.6	1660	28	1040	6
4.1	435	220	0.52	57.2	0.08	0.0702	0.9	1.478	1.0	0.1527	0.5	934	18	916	4
5.1	2082	25	0.01	268.6	0.04	0.0690	0.7	1.429	0.7	0.1501	0.2	900	14	902	2
6.1	1057	33	0.03	139.0	0.04	0.0694	0.8	1.463	0.9	0.1529	0.3	910	16	917	3
7.1	1074	38	0.04	142.5	0.07	0.0699	0.6	1.488	2.1	0.1543	2.0	927	12	925	17
8.1	1176	25	0.02	151.4	0.10	0.0746	2.5	1.541	3.1	0.1497	1.7	1059	50	900	15
8.2	754	33	0.05	99.4	0.20	0.0724	1.3	1.530	1.5	0.1533	0.8	997	26	919	7
9.1	1107	47	0.04	153.5	1.48	0.1089	3.7	2.388	3.7	0.1590	0.3	1782	67	951	3
10.1	1269	142	0.12	171.9	1.01	0.0906	3.3	1.950	3.3	0.1560	0.5	1439	62	935	4
11.1	953	39	0.04	122.4	0.14	0.0768	0.9	1.580	1.3	0.1492	0.9	1115	19	897	7

TABLE 5
(continued)

Spot	U (ppm)	Th (ppm)	Th/U	Pb* (ppm)	Common ^{206}Pb(%)	Isotopic Ratios						Ages			
						$^{207}Pb/^{206}Pb$	±σ (%)	$^{207}Pb/^{235}U$	±σ (%)	$^{206}Pb/^{238}U$	±σ (%)	$^{207}Pb/^{206}Pb$	±σ	$^{206}Pb/^{238}U$	±σ
Sample 41-1 (Hamm Peak)															
Oscillatory-zoned core															
12.1	1034	167	0.17	136.1	0.10	0.0701	1.4	1.480	1.7	0.1530	1.0	932	29	918	9
13.1	1667	266	0.17	231.6	0.05	0.0701	0.8	1.563	0.9	0.1617	0.3	932	17	966	3
13.2	2658	113	0.04	386.1	0.01	0.0761	0.4	1.774	0.5	0.1691	0.3	1098	7	1007	3
Bright planar- and sector-zoned rim															
14.1	322	167	0.53	41.1	0.19	0.0665	1.2	1.360	1.3	0.1482	0.5	824	26	891	4
15.1	436	210	0.50	55.1	0.15	0.0681	1.0	1.379	1.1	0.1470	0.4	870	21	884	4
16.1	409	188	0.47	51.8	0.13	0.0696	1.1	1.413	1.2	0.1472	0.5	917	22	885	4
16.2	271	137	0.52	33.0	0.65	0.0798	2.2	1.548	2.3	0.1407	0.7	1192	43	849	5
17.1	357	180	0.52	45.4	0.15	0.0750	1.1	1.525	1.4	0.1475	0.9	1068	21	887	7
18.1	458	187	0.42	57.3	0.20	0.0681	1.2	1.365	1.6	0.1454	1.0	870	24	875	8
19.1	429	199	0.48	54.2	0.04	0.0689	0.9	1.398	1.1	0.1470	0.5	897	19	884	5
20.1	453	224	0.51	56.7	0.21	0.0699	1.9	1.399	1.9	0.1452	0.5	926	38	874	4
21.1	390	179	0.47	49.1	0.09	0.0734	1.7	1.482	1.8	0.1464	0.5	1025	35	881	4
22.1	378	182	0.50	46.9	0.39	0.0725	1.6	1.437	1.6	0.1438	0.5	1000	32	866	4
23.1	386	67	0.18	49.6	0.26	0.0680	1.3	1.398	1.4	0.1491	0.6	869	26	896	5
24.1	303	78	0.27	38.4	0.42	0.0658	1.8	1.333	1.9	0.1469	0.6	800	39	883	5
Sample 82-1 (Statler Hills)															
Oscillatory-zoned core															
1.1	448	295	0.68	72.2	0.53	0.0778	2.3	2.002	2.4	0.1866	0.6	1143	46	1103	6
2.1	241	179	0.77	31.6	0.62	0.0743	2.5	1.556	2.6	0.1518	0.7	1051	51	911	6
3.1	401	302	0.78	66.0	0.10	0.0770	0.9	2.032	1.1	0.1914	0.5	1122	19	1129	5
4.1	278	149	0.56	47.2	0.13	0.0794	1.3	2.161	1.4	0.1974	0.6	1182	25	1161	7
5.1	186	124	0.69	31.2	0.18	0.0793	1.4	2.126	1.6	0.1944	0.8	1179	28	1145	8
6.1	242	249	1.06	34.8	0.12	0.0726	1.4	1.676	1.6	0.1675	0.7	1002	28	998	7
7.1	167	76	0.47	24.7	0.00	0.0745	1.6	1.772	1.8	0.1725	0.8	1055	31	1026	8
8.1	254	141	0.57	43.1	0.58	0.0775	2.1	2.096	2.2	0.1961	0.7	1134	42	1154	7
9.1	331	316	0.99	56.1	0.08	0.0799	5.3	2.173	5.3	0.1973	0.6	1194	104	1161	6
10.1	497	284	0.59	80.7	0.05	0.0794	0.8	2.068	1.0	0.1889	0.5	1182	17	1115	5
11.1	221	100	0.47	32.3	0.24	0.0748	2.3	1.757	2.4	0.1703	0.8	1064	46	1014	8
12.1	349	203	0.60	59.6	0.22	0.0776	1.3	2.120	1.4	0.1982	0.6	1136	25	1166	6

TABLE 5
(continued)

Spot	U (ppm)	Th (ppm)	Th/U	Pb* (ppm)	Common ^{206}Pb(%)	Isotopic Ratios						Ages			
						$^{207}Pb/^{206}Pb$	±σ (%)	$^{207}Pb/^{235}U$	±σ (%)	$^{206}Pb/^{238}U$	±σ (%)	$^{207}Pb/^{206}Pb$	±σ	$^{206}Pb/^{238}U$	±σ
Sample 82-1 (Statler Hills)															
Oscillatory-zoned core															
13.1	362	230	0.65	57.0	0.18	0.0756	2.0	1.906	2.2	0.1828	0.9	1085	40	1082	9
14.1	311	171	0.57	45.5	0.73	0.0778	2.6	1.814	2.7	0.1691	0.6	1141	52	1007	6
15.1	385	386	1.03	61.5	0.06	0.0775	2.3	1.985	2.4	0.1857	0.6	1135	47	1098	6
16.1	307	307	1.03	39.3	0.22	0.0711	1.6	1.459	1.7	0.1487	0.6	961	33	894	5
17.1	291	301	1.07	46.5	0.16	0.0788	1.4	2.021	1.5	0.1861	0.6	1166	27	1100	6
18.1	191	124	0.67	33.2	0.43	0.0763	2.1	2.117	2.2	0.2011	0.8	1104	42	1181	9
Bright planar- and fir-tree-zoned rim															
19.1	329	51	0.16	24.1	0.33	0.0553	2.8	0.649	2.9	0.0851	0.7	425	63	527	3
20.1	338	106	0.32	24.9	-0.07	0.0575	1.9	0.680	2.0	0.0857	0.7	511	42	530	3
21.1	369	121	0.34	27.3	0.17	0.0572	2.4	0.678	2.5	0.0859	0.7	499	52	531	3
21.2	307	101	0.34	22.4	0.20	0.0556	2.5	0.648	2.6	0.0846	0.7	436	55	523	4
22.1	349	54	0.16	27.0	0.13	0.0583	1.8	0.722	1.9	0.0899	0.7	541	40	555	4
Sample 117-2 (Jennings Promontory)															
Oscillatory-zoned core															
1.1	417	222	0.55	70.5	0.25	0.0794	4.5	2.151	5.8	0.1964	3.6	1183	89	1156	38
2.1	3683	315	0.09	481.6	0.01	0.0745	0.3	1.563	0.4	0.1522	0.2	1054	7	913	2
3.1	409	140	0.35	54.0	0.26	0.0841	3.2	1.781	3.2	0.1535	0.5	1295	62	921	5
4.1	209	510	2.52	14.7	0.41	0.0540	4.1	0.607	4.1	0.0815	0.9	369	91	505	4
5.1	406	249	0.63	43.1	0.19	0.0687	1.9	1.167	2.0	0.1232	0.6	891	40	749	4
6.1	320	186	0.60	40.7	0.22	0.0709	1.6	1.444	2.2	0.1477	1.4	955	34	888	12
7.1	380	510	1.39	61.8	0.04	0.0758	1.0	1.977	1.6	0.1892	1.3	1089	21	1117	13
8.1	322	133	0.43	23.2	0.07	0.0608	1.8	0.703	1.9	0.0838	0.7	633	38	519	4
9.1	295	253	0.88	44.3	0.64	0.0755	4.1	1.806	4.1	0.1735	0.7	1082	81	1031	7
10.1	1255	554	0.46	165.6	0.06	0.0769	0.5	1.628	0.6	0.1535	0.3	1120	11	921	3
11.1	3002	417	0.14	469.4	0.01	0.0758	0.4	1.901	0.5	0.1820	0.3	1089	8	1078	3
12.1	318	251	0.82	40.6	0.29	0.0726	1.9	1.484	2.0	0.1482	0.6	1003	40	891	5
13.1	722	268	0.38	92.0	0.10	0.0730	1.2	1.494	1.3	0.1483	0.4	1015	24	891	3
14.1	620	289	0.48	90.0	0.07	0.0796	0.9	1.853	1.0	0.1688	0.5	1188	18	1005	5
15.1	563	413	0.76	70.9	0.18	0.0740	1.1	1.493	1.3	0.1463	0.6	1042	23	880	5
16.1	673	428	0.66	83.0	0.19	0.0721	1.1	1.424	1.1	0.1433	0.4	988	21	863	3

TABLE 5
(continued)

Spot	U (ppm)	Th (ppm)	Th/U	Pb* (ppm)	Common ^{206}Pb(%)	Isotopic Ratios						Ages			
						^{207}Pb/^{206}Pb	±σ (%)	^{207}Pb/^{235}U	±σ (%)	^{206}Pb/^{238}U	±σ (%)	^{207}Pb/^{206}Pb	±σ	^{206}Pb/^{238}U	±σ
Sample 117-2 (Jennings Promontory)															
Oscillatory-zoned core															
17.1	835	403	0.50	123.6	0.06	0.0735	0.7	1.746	0.8	0.1723	0.4	1027	14	1025	4
18.1	3300	524	0.16	424.8	0.04	0.0738	0.8	1.525	0.9	0.1498	0.3	1037	17	900	2
Bright fir-tree-zoned rim															
2.2	195	314	1.66	13.9	0.21	0.0556	2.8	0.633	3.0	0.0826	0.9	435	63	512	4
8.2	74	118	1.64	5.2	0.00	0.0633	3.6	0.708	3.9	0.0812	1.4	718	77	503	7
9.2	169	243	1.48	12.0	0.24	0.0560	2.7	0.635	2.9	0.0822	0.9	453	60	509	5
11.2	100	141	1.46	7.1	0.44	0.0657	7.7	0.749	7.8	0.0826	1.2	798	161	512	6
19.1	101	134	1.37	7.1	0.00	0.0576	3.3	0.647	3.5	0.0813	1.2	516	72	504	6
20.1	101	154	1.59	7.3	0.00	0.0524	3.5	0.606	3.7	0.0839	1.2	303	80	519	6
21.1	105	147	1.47	7.3	0.29	0.0531	4.0	0.602	4.2	0.0822	1.2	334	91	509	6
22.1	104	151	1.50	7.3	0.00	0.0544	3.3	0.609	3.5	0.0813	1.2	386	75	504	6
23.1	129	194	1.56	9.3	0.34	0.0534	4.9	0.616	5.0	0.0837	1.1	345	110	518	5
24.1	132	188	1.48	9.4	0.17	0.0508	4.0	0.581	4.2	0.0831	1.1	231	93	514	5
25.1	108	158	1.51	7.8	0.00	0.0577	3.3	0.669	3.5	0.0842	1.2	517	73	521	6
26.1	97	147	1.57	7.0	0.70	0.0528	5.1	0.611	5.2	0.0839	1.3	320	115	520	6
27.1	90	120	1.37	6.5	0.40	0.0570	4.4	0.655	4.6	0.0833	1.3	491	97	516	6
28.1	101	150	1.54	7.2	0.28	0.0530	4.8	0.606	5.0	0.0830	1.2	327	110	514	6
Sample 150-1 (Luff Nunatak)															
Oscillatory-zoned core															
1.1	190	53	0.29	24.1	0.31	0.0712	4.3	1.441	4.8	0.1468	2.1	963	89	883	18
2.1	282	159	0.58	57.6	0.24	0.0864	1.2	2.827	1.6	0.2373	1.1	1347	23	1373	14
3.1	541	270	0.52	109.5	0.12	0.0858	1.1	2.781	1.7	0.2352	1.3	1333	22	1362	15
4.1	248	135	0.56	50.1	0.32	0.0885	1.5	2.858	1.7	0.2342	0.7	1393	29	1357	9
5.1	451	210	0.48	88.8	0.24	0.0878	1.0	2.770	1.1	0.2289	0.5	1377	19	1329	6
6.1	386	260	0.70	75.0	0.04	0.0843	0.9	2.626	1.1	0.2258	0.6	1300	17	1313	7
7.1	527	202	0.40	116.2	0.06	0.0895	0.7	3.167	0.8	0.2566	0.5	1415	13	1472	6
8.1	381	123	0.33	39.1	0.60	0.0690	3.1	1.129	3.2	0.1187	0.6	897	64	723	4
9.1	1223	315	0.27	133.6	0.09	0.0721	2.1	1.262	2.2	0.1270	0.4	987	43	771	3
10.1	345	211	0.63	67.6	0.52	0.0848	2.1	2.652	2.2	0.2268	0.6	1311	41	1318	7

TABLE 5
(continued)

Spot	U (ppm)	Th (ppm)	Th/U	Pb* (ppm)	Common ^{206}Pb(%)	Isotopic Ratios						Ages			
						$\frac{^{207}Pb}{^{206}Pb}$	±σ (%)	$\frac{^{207}Pb}{^{235}U}$	±σ (%)	$\frac{^{206}Pb}{^{238}U}$	±σ (%)	$\frac{^{207}Pb}{^{206}Pb}$	±σ	$\frac{^{206}Pb}{^{238}U}$	±σ
Sample 150-1 (Luff Nunatak))															
Oscillatory-zoned core															
11.1	675	315	0.48	135.1	0.05	0.0875	0.9	2.809	1.0	0.2328	0.5	1372	17	1349	6
12.1	715	258	0.37	120.5	0.04	0.0871	1.0	2.356	1.2	0.1961	0.5	1364	20	1154	5
13.1	208	89	0.44	31.0	0.37	0.0857	3.0	2.037	3.2	0.1723	1.2	1332	58	1025	11
14.1	279	100	0.37	57.7	0.25	0.0857	2.4	2.839	2.5	0.2403	0.7	1331	46	1388	8
15.1	466	271	0.60	94.8	0.02	0.0861	0.8	2.808	1.2	0.2367	0.9	1340	15	1369	12
16.1	510	205	0.42	91.4	0.15	0.0804	2.9	2.309	2.9	0.2082	0.5	1208	56	1219	6
17.1	550	196	0.37	98.4	0.18	0.0830	1.5	2.380	1.6	0.2079	0.5	1270	30	1218	5
18.1	1034	437	0.44	169.3	0.04	0.0854	0.8	2.243	0.9	0.1905	0.5	1325	15	1124	5
Bright planar- and sector-zoned rim															
19.1	170	244	1.48	18.2	0.31	0.0676	2.6	1.157	2.7	0.1242	0.9	855	53	755	6
20.1	667	210	0.33	82.6	0.14	0.0649	1.2	1.288	1.3	0.1439	0.5	771	25	867	4
21.1	223	350	1.62	28.9	0.34	0.0699	4.7	1.448	6.6	0.1502	4.6	926	97	902	39
22.1	187	317	1.75	24.0	0.30	0.0714	2.0	1.464	2.2	0.1488	0.9	969	40	894	8
23.1	554	242	0.45	73.4	0.07	0.0701	2.4	1.490	2.4	0.1541	0.5	932	49	924	4
24.1	199	296	1.54	26.5	0.16	0.0746	1.9	1.588	2.1	0.1544	0.8	1058	39	925	7
25.1	201	31	0.16	14.8	0.45	0.0592	3.0	0.698	3.1	0.0855	0.9	574	65	529	4
26.1	182	293	1.66	24.0	0.06	0.0704	2.7	1.489	2.9	0.1535	1.1	939	56	921	9
27.1	194	327	1.74	20.5	0.38	0.0703	5.7	1.185	5.7	0.1223	0.9	937	116	744	6
28.1	278	125	0.47	32.3	0.92	0.0710	4.8	1.312	4.9	0.1340	0.8	958	98	810	6
29.1	172	249	1.50	21.7	0.70	0.0691	6.3	1.390	6.3	0.1458	0.9	903	129	878	7
30.1	308	158	0.53	36.6	0.15	0.0701	1.7	1.336	2.0	0.1383	1.1	930	35	835	9

Pb*denotes radiogenic Pb. Common ^{206}Pb(%) represents the proportion of common ^{206}Pb in total ^{206}Pb measured. Common Pb was corrected using the measured ^{204}Pb. All uncertainties are 1σ.

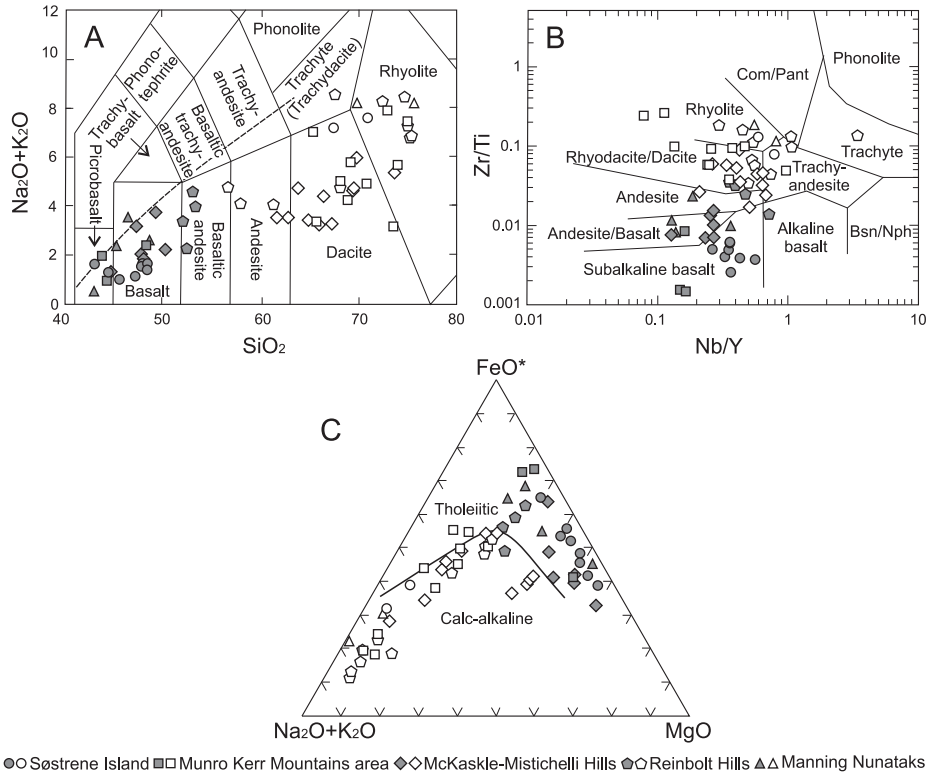

Fig. 3. (A) Total alkali vs. SiO_2 (TAS) diagram for classification of mafic granulites and felsic orthogneisses (after Middlemost, 1994). The dashed line represents the boundary between alkaline (upper) and subalkaline (lower). (B) Zr/Ti vs. Nb/Y diagram for classification of mafic granulites and felsic orthogneisses (after Winchester and Floyd, 1977). (C) Alkali-FeO*-MgO (AFM) diagram of mafic granulites and felsic orthogneisses (after Irvine and Baragar, 1971). Solid symbols indicate mafic granulites and open symbols indicate felsic orthogneisses.

calc-alkaline trend except two (samples 35-1 and 38-7) from the Munro Kerr Mountains area in the tholeiitic trend (see fig. 3C). The rocks are metaluminous to peraluminous, with ASI values [molar $Al_2O_3/(CaO + Na_2O + K_2O)$] less than 1.1 for most samples, which match the compositions of I-type granites (fig. 5A). However, 6 garnet-rich samples (31-2, 35-1, 38-7, 43-8, 41-1 and 41-4) from the Munro Kerr Mountains area have ASI > 1.1, analogous to S-type granites. The $10^4Ga/Al$ ratios of the rocks range from 1.71 to 2.92, with an average of 2.45. Although the $Na_2O + K_2O$ contents and FeO*/MgO ratios (1.01-5.32, except sample 150-1) of most samples are consistent with their being I- and S-type granites, some samples nevertheless fall in the A-type granite field due to the enrichment of Ga, Zr, Nb and Y (Whalen and others, 1987) (fig. 5B). Since these samples, except two with relatively lower SiO_2 contents (56.02 and 57.31 wt%), are highly fractionated (fig. 5C), we infer that they were fractionated I- or S-type granites. In addition, 7 samples, including the oldest 38-1 from the Hamm Peak, 72-7 and 81-7 from the McKaskle-Mistichelli Hills, and 129-1, 135-1, 136-1 and 141-1 from the Reinbolt Hills, are strongly depleted in Y (1.33-10.8 ppm). They have Sr/Y ratios >40 (except 81-7 with Sr/Y = 33), belonging to high Sr/Y granites (fig. 5D). In particular, 4 such samples from the Reinbolt Hills typically show a partial melting trend (see fig. 5C).

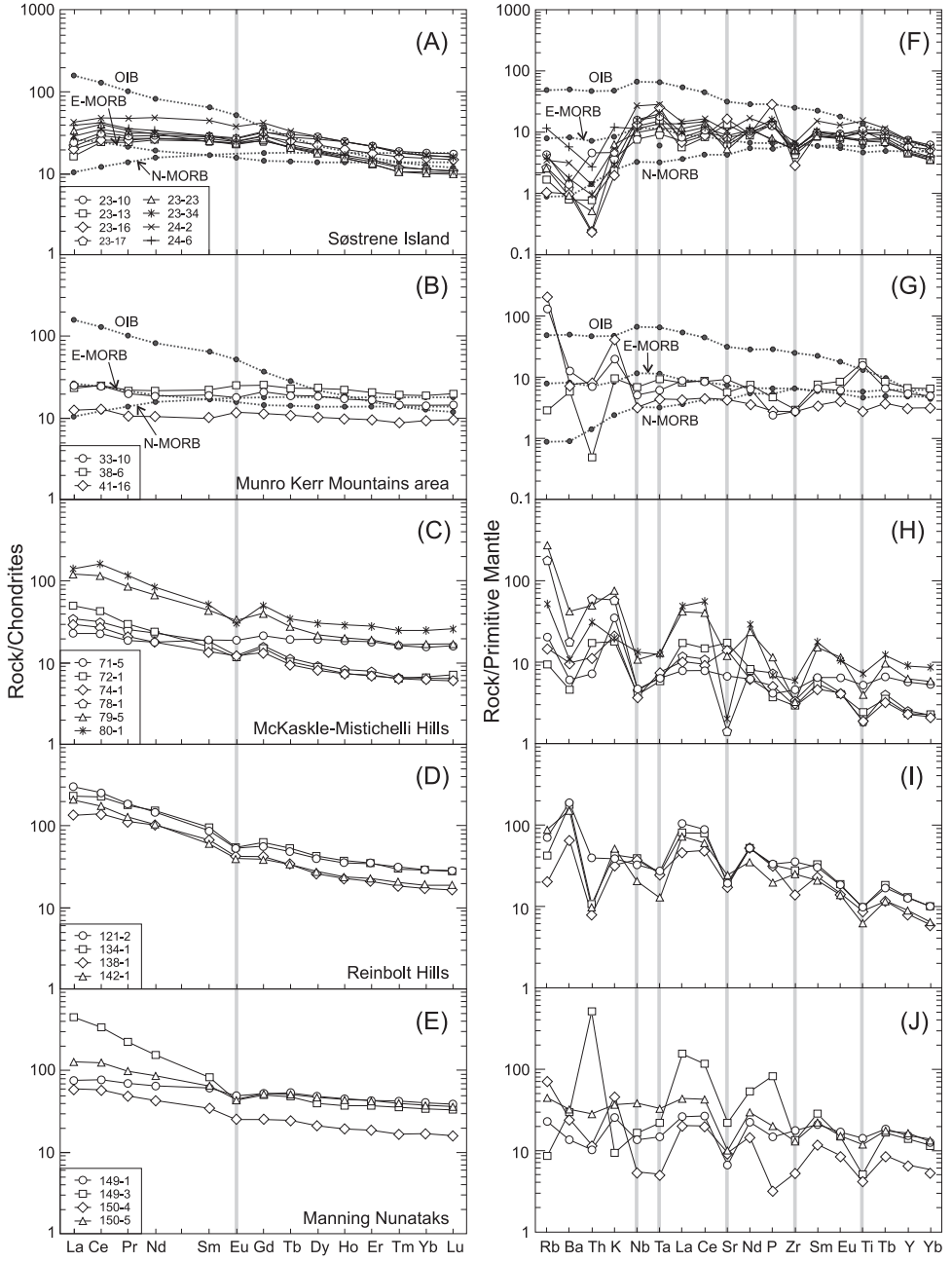

Fig. 4. Chondrite-normalized REE patterns (A-E) and primitive mantle (PM) normalized spidergrams (F-J) of mafic granulites. OIB, E-MORB and N-MORB data and chondrite and PM values used for normalization are from Sun and McDonough (1989).

The REE patterns of high Sr/Y orthogneisses are moderately or strongly fractionated [$(La/Yb)_N$ = 13-88] and typically depleted in HREE. They have total REE contents of 30 to 117 ppm and all show marked positive Eu anomalies (Eu/Eu* =

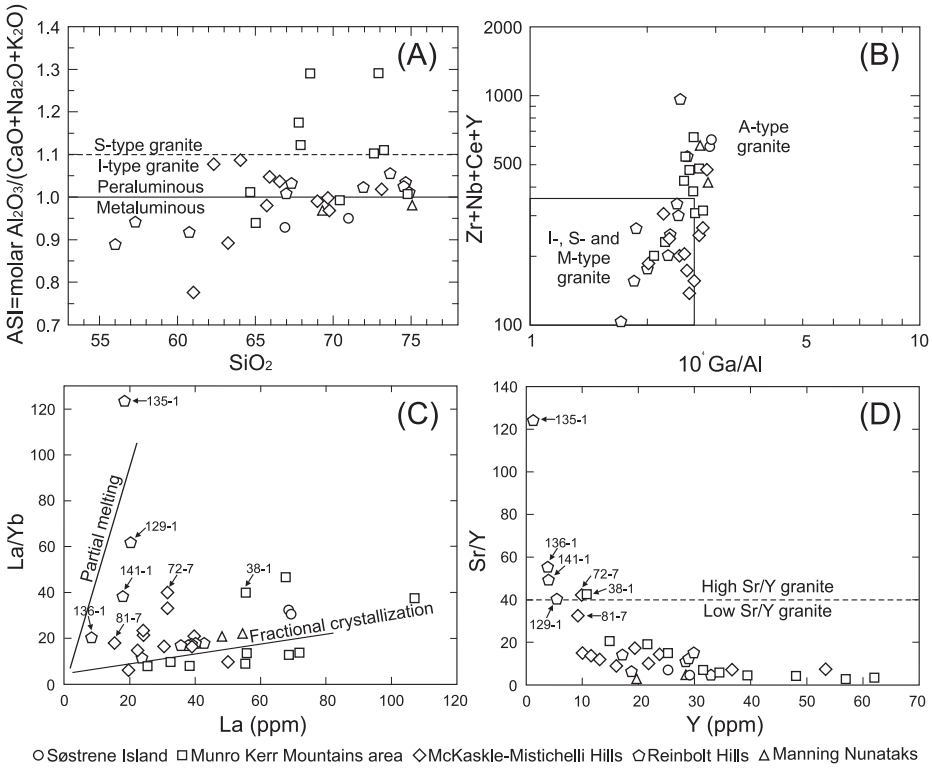

Fig. 5. Diagrams illustrating the chemical characteristics of felsic orthogneisses. (A) ASI [molar $Al_2O_3/(CaO + Na_2O + K_2O)$] vs. SiO_2 diagram. (B) $10^4Ga/Al$ vs. Zr + Nb + Ce + Y diagram (after Whalen and others, 1987). (C) La/Yb-La diagram. (D) Sr/Y-Y diagram.

1.47-5.05). Other felsic orthogneisses display moderately LREE-enriched patterns (figs. 6A-6E), with $(La/Yb)_N$ ratios of 4 to 33 and total REE contents of 103 to 452 ppm. Most samples have negative Eu anomalies (Eu/Eu* = 0.38-0.90), but some (samples 41-1, 72-5, 74-8 and 79-1) show no Eu anomalies (Eu/Eu* = 0.96-1.10), or even a positive Eu anomaly (sample 37-3: Eu/Eu* = 1.37). In the spidergrams (figs. 6F-6J), all the felsic orthogneisses exhibit high abundances of Rb, Ba, K, Zr and La (REE), and relative depletion in Nb, Ta, P, Ti and Sr, except for the high Sr/Y gneisses. The high Sr/Y orthogneisses commonly show no depletion in Sr, or even show a small positive Sr anomaly.

Nd Isotopes

Based on the available zircon U-Pb age data (Liu and others, 2007a, 2009a; Grew and others, 2012; this paper), the initial ε_{Nd} values [$\varepsilon_{Nd}(T)$] were calculated at 1350, 1200, 1150, and 1050 Ma for samples from different localities. Overall, Group I-II mafic granulites display $\varepsilon_{Nd}(T)$ values from +4.1 to −0.4, whereas most Group III mafic granulites show negative $\varepsilon_{Nd}(T)$ values from −3.2 to −4.7 (fig. 7). However, three Group III samples (71-5, 149-1 and 150-4) have higher $\varepsilon_{Nd}(T)$ values (+3.4, +0.6 and −1.2). Nd model ages (T_{DM}) of samples with negative $\varepsilon_{Nd}(T)$ values are mainly between 2.25 and 1.89 Ga (except sample 78-1 with T_{DM} = 2.48 Ga). Other samples

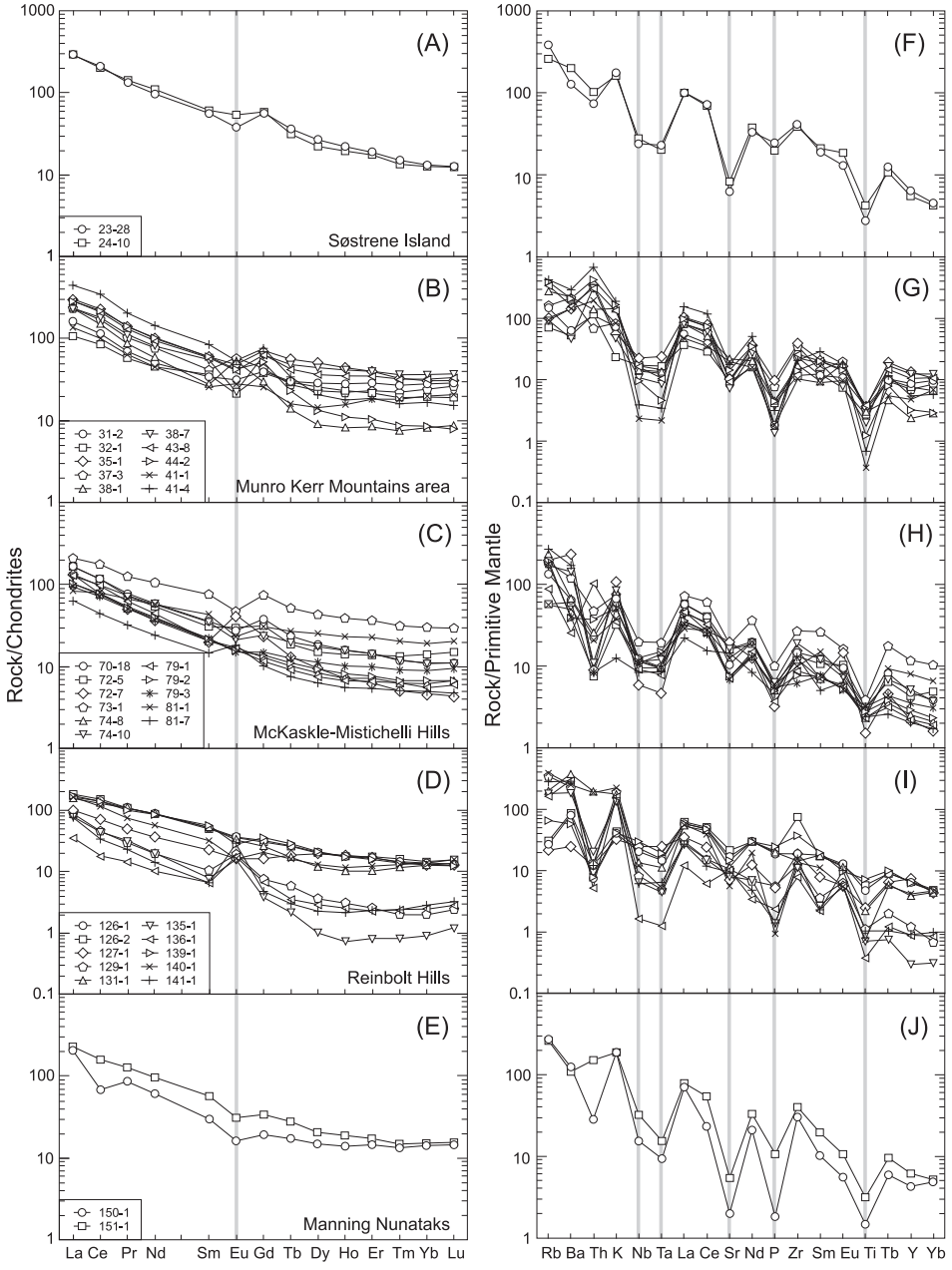

Fig. 6. Chondrite-normalized REE patterns (A-E) and primitive mantle (PM) normalized spidergrams (F-J) of felsic orthogneisses. Chondrite and PM values used for normalization are from Sun and McDonough (1989).

yielded insignificant T_{DM} ages since their $f_{Sm/Nd}$ values are greater than -0.2 (Jahn and others, 2000). Felsic orthogneisses have $\varepsilon_{Nd}(T)$ values from -2.4 to -7.6, and T_{DM} model ages of 2.23 to 1.85 Ga (except samples 32-1 and 38-7 yielding slightly older ages).

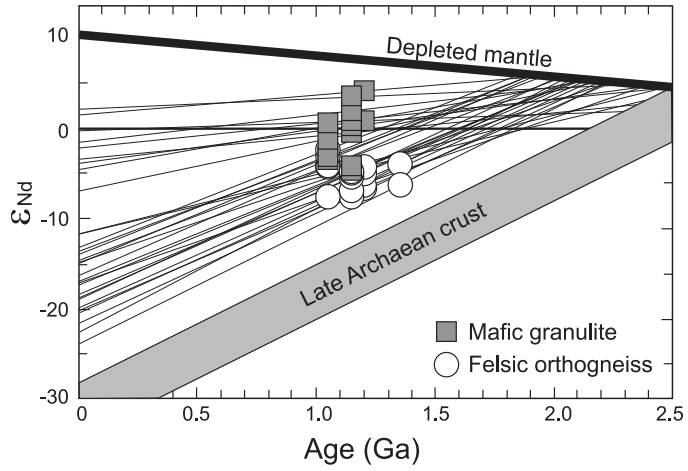

Fig. 7. Nd evolution diagram for mafic granulites and felsic orthogneisses.

U-Pb Zircon Ages

Zircon grains from sample 24-10 are prismatic, with lengths of 200 to 400 μm and length to width ratios of 2 to 4. The CL images reveal that most grains have core-rim structures, characterized by oscillatory zoning in the core and bright homogeneous or planar zoning in the rim. However, the oscillatory bands of some cores have been thickened and even homogenized as a consequence of solid-state recrystallization. Twenty-six core analyses yielded a very large range of $^{206}Pb/^{238}U$ ages from 1178 ± 8 to 597 ± 4 Ma (fig. 8A), with Th/U ratios ranging from 0.18 to 5.19. Of them 11 old data points produced a weighted mean $^{207}Pb/^{206}Pb$ age of 1117 ± 37 Ma (MSWD = 2.8). This age is considered to be the minimum protolith age of the felsic orthogneiss. Fifteen rim analyses also yielded scattered $^{206}Pb/^{238}U$ ages from 1159 ± 10 Ma to 719 ± 5 Ma. Most of these ages are discordant, with Th/U ratios varying from 0.34 to 6.12. Among them, 4 relatively young data points gave a weighted mean $^{206}Pb/^{238}U$ age of 922 ± 10 Ma (MSWD = 0.86). This age may reflect the time of metamorphism.

Zircon grains from sample 31-2 are ovoid or short prismatic, with lengths ranging from 100 to 250 μm. Most grains show an oscillatory-zoned core, a dark planar- or sector-zoned mantle and a very narrow bright rim, which cannot be analyzed. Two analyses of cores produced old $^{207}Pb/^{206}Pb$ ages of 1971 ± 10 and 1580 ± 18 Ma. Sixteen other core analyses, except for 1 deviated spot, plot on or near a discordia, yielding an upper intercept age of 1327 ± 29 Ma and a lower intercept age of 542 ± 190 Ma (MSWD = 2.1) (fig. 8B). Their Th/U ratios vary from 0.33 to 1.03. Fifteen rim analyses are mostly discordant and show low Th/U ratios (0.01-0.13). Of them 8 data points gave a weighted mean $^{207}Pb/^{206}Pb$ age of 997 ± 27 Ma (MSWD = 1.4). Taking into account the CL features and Th/U ratios of the dated zircon domains, we interpret the age of 1327 ± 29 Ma as a protolith age, and the age of 997 ± 27 Ma as a metamorphic age.

Larger zircon grains from sample 41-1 are prismatic, whereas smaller grains are rounded to ovoid. The sizes of all grains range from 100 to 300 μm. All grains show simple zoning with oscillatory-zoned core and bright planar- or sector-zoned rim, but most cores have been homogenized and, in some cases, partially blurred. Among 15 core analyses, 3 fine-scale oscillatory-zoned cores yielded an upper intercept age of 1079 ± 29 Ma (MSWD = 0.16) (fig. 8C). Six homogenous cores produced a weighted

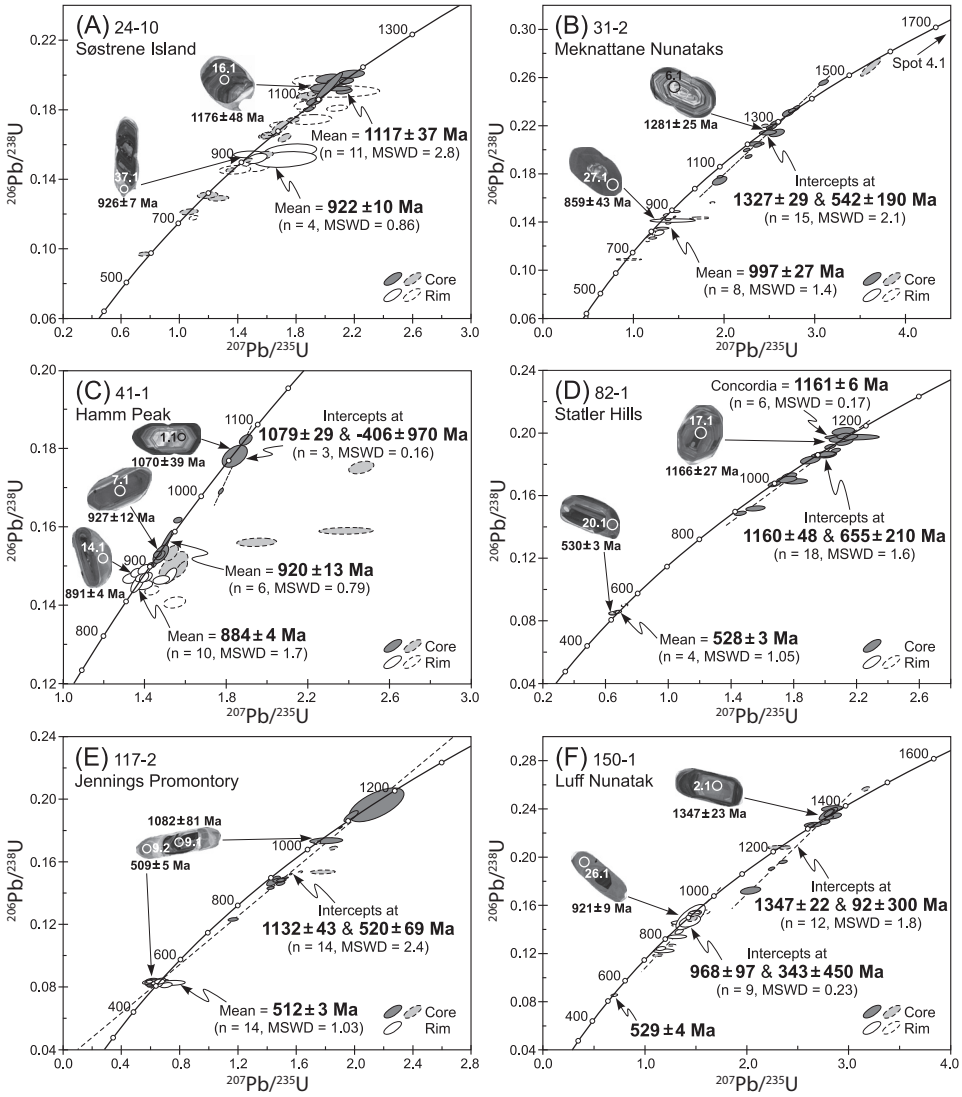

Fig. 8. Zircon U-Pb concordia diagrams of felsic orthogneisses, with inset showing CL images of zircon. Circles on zircon represent SHRIMP analytical spots, with diameters of ~30 μm.

mean $^{207}Pb/^{206}Pb$ age of 920 ± 13 Ma (MSWD = 0.79). The remaining 6 spots gave highly discordant ages. Th/U ratios for different cores are variable from 0.01 to 0.74. Ten rim analyses are tightly clustered with a weighted mean $^{206}Pb/^{238}U$ age of 884 ± 4 Ma (MSWD = 1.7). Two other spots show younger ages due to Pb loss. Th/U ratios for the rims range from 0.18 to 0.53. The age of 1079 ± 29 Ma is interpreted as the emplacement age of the felsic orthogneiss protolith, whereas the ages of 920 ± 13 and 884 ± 4 Ma as a recrystallization age and a metamorphic age, respectively.

Zircon grains from sample 82-1 are ovoid or prismatic, with lengths varying from 100 to 450 μm. All grains display oscillatory zoning. Some of them have a bright planar- or fir-tree-zoned overgrowth rim. Eighteen core analyses fall on or near a discordia

with upper and lower intercept ages at 1160 ± 48 and 655 ± 210 Ma, respectively (MSWD = 1.6) (fig. 8D). Their Th/U ratios are between 0.47 and 1.07. Of them 6 old data points produced a concordant age of 1161 ± 6 Ma (MSWD = 0.17). The age is interpreted as the protolith age of the felsic orthogneiss. Among 5 rim analyses, except for 1 spot shows a slightly older age, others yielded a weighted mean $^{206}Pb/^{238}U$ age of 528 ± 3 Ma (MSWD = 1.05). Th/U ratios for these zircon domains range from 0.16 to 0.34. This age is taken to date the time of metamorphism.

Zircon grains from sample 117-2 are long prismatic, 150 to 400 μm in length, and length to width ratios of 2 to 5. Almost all grains show typical core-rim structures. Eighteen analyses on oscillatory-zoned cores yielded $^{206}Pb/^{238}U$ ages from 1156 ± 38 to 519 ± 4 Ma, with Th/U ratios of 0.09 to 2.52. Excluding 4 deviated spots, the others fall on a discordia with an upper intercept age of 1132 ± 43 Ma and a lower intercept age of 520 ± 69 Ma (MSWD = 2.4) (fig. 8E). The data for 14 bright fir-tree-zoned overgrowths are tightly grouped, yielding a mean $^{206}Pb/^{238}U$ age of 512 ± 3 Ma (MSWD = 1.03). Their Th/U ratios are concentrated to 1.37 to 1.66. The ages of 1132 ± 43 and 512 ± 3 Ma are considered to represent the protolith age and metamorphic age, respectively.

Zircon grains from sample 150-1 are ovoid or short prismatic, with sizes ranging from 100 to 300 μm. Most grains have an oscillatory-zoned core and a bright planar- or sector-zoned rim. However, many cores have been severely blurred due to solid-state recrystallization. Among 18 core analyses, 12 form a discordant array with an upper intercept age of 1347 ± 22 Ma (MSWD = 1.8). This is in agreement within error with the weighted mean $^{207}Pb/^{206}Pb$ age of 1344 ± 12 Ma (MSWD = 1.7) (fig. 8F). Six others gave a scattered age pattern from 1415 ± 13 Ma ($^{207}Pb/^{206}Pb$ age) to 723 ± 4 Ma ($^{206}Pb/^{238}U$ age). Th/U ratios for core domains range from 0.27 to 0.70. The age of 1347 ± 22 Ma is interpreted as the protolith age of the felsic orthogneiss. Among 12 rim analyses, except for 2 outliers and spot 25.1, 9 data points fall on a discordia, with an upper intercept age of 968 ± 97 Ma (MSWD = 0.23), slightly older than the weighted mean $^{207}Pb/^{206}Pb$ age of 931 ± 37 Ma (MSWD = 0.39). Their Th/U ratios vary from 0.33 to 1.75. The age of 968 ± 97 is taken as the time of early Neoproterozoic metamorphic event. Spot 25.1 yielded the youngest $^{206}Pb/^{238}U$ age of 529 ± 4 Ma, with Th/U ratio of 0.16, probably reflecting the effect of Cambrian metamorphism.

DISCUSSION

Element Mobility During Granulite Facies Metamorphism

The behavior of trace elements during high-grade metamorphism has received much attention. It has been widely accepted that most granulite facies rocks are variably depleted in LILE, particularly K, Rb, Th and U, with concurrent increases in K/Rb and Th/U ratios (for example, Heier, 1973; Tarney and Windley, 1977; Jahn and Zhang, 1984; Sheraton and Collerson, 1984; Rudnick and others, 1985; Jahn, 1990; Rudnick and Presper, 1990). However, some post-Archean granulite terranes were also documented to have not experienced significant LILE depletion, with the possible exception of U (for example, Barbey and Cuney, 1982; Sheraton and Black, 1983; Stephenson, 2000). Mafic granulites and felsic orthogneisses from the eastern Amery Ice Shelf-southwestern Prydz Bay area have undergone two granulite facies metamorphic cycles during the periods ~1000 to 900 and ~550 to 500 Ma (Liu and others, 2013). Therefore, we need to understand the trace element mobility during metamorphism before discussing petrogenesis and tectonic setting.

Most felsic orthogneisses, except samples 126-1, 126-2 and 127-1 from the Reinbolt Hills, have K/Rb ratios between 100 and 390, with an average of 215. This matches the main trend of continental granitoids (MT; Shaw, 1968) (fig. 9A). Their Rb/Sr ratios are more than 0.1 (fig. 9B). The 3 exceptional samples show slightly higher K/Rb

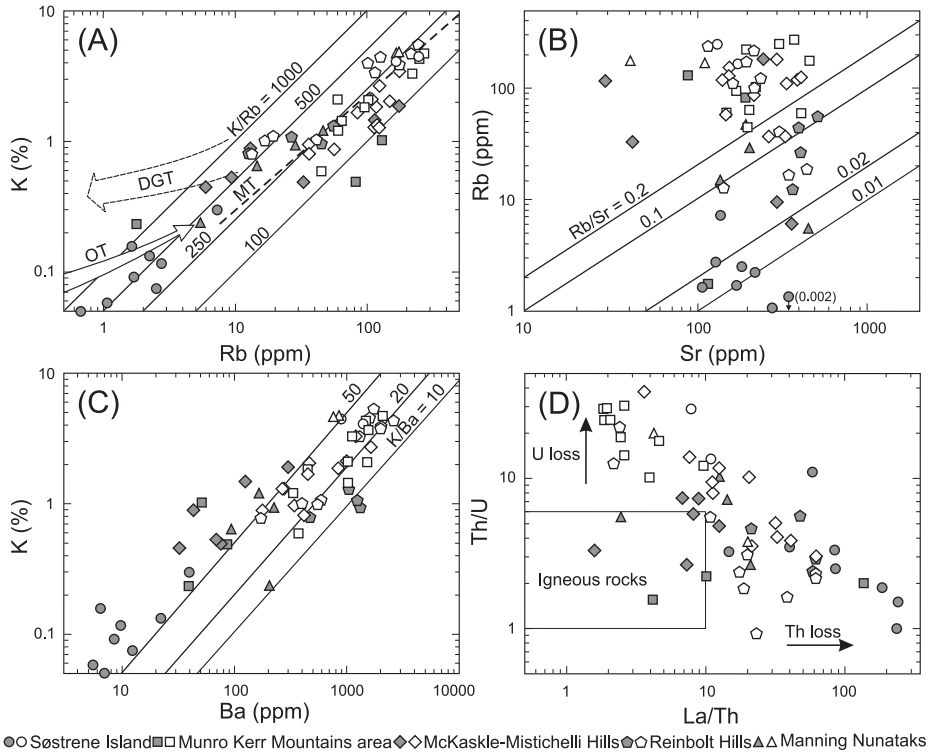

Fig. 9. Diagrams illustrating the element mobility during granulite facies metamorphism. (A) K-Rb diagram. OT (oceanic trend of MORB) and MT (main trend of continental granitoids) are given by Shaw (1968). DGT (depleted granulite trend) is given by Jahn (1990). (B) Rb-Sr diagram. (C) K-Ba diagram. (D) Th/U-La/Th diagram. The box represents the field of common igneous rocks (after Rudnick and Presper, 1990). Solid symbols indicate mafic granulites and open symbols indicate felsic orthogneisses.

ratios (560-600) and lower Rb/Sr ratios (<0.1), probably implying some, but not much, loss of Rb relative to K and Sr during metamorphism. Therefore, the data do not follow the depleted granulite trend (DGT, fig. 9A) reported by Jahn (1990). The average K/Ba and Rb/Ba ratios for all felsic orthogneisses are 30 and 0.14, respectively (fig. 9C), further suggesting little mobility of K, Rb and Ba. The case is very similar to granulite facies rocks from the northern Prince Charles Mountains (Sheraton and Black, 1983; Munksgaard and others, 1992; Sheraton and others, 1996; Stephenson, 2000). However, La/Th and Th/U ratios for the felsic orthogneisses from the studied area do not lie within the normal range of igneous rocks (fig. 9D), indicating that both Th and U were depleted during metamorphism.

In contrast, mafic granulites show highly variable concentrations of K, Rb, Sr and Ba, with K/Rb = 60–1310, Rb/Sr = 0.002–1.45, K/Ba = 7–250, and Rb/Ba = 0.02–2.52 (see figs. 9A-9C). For the low-K (K_2O = 0.06-0.36 wt%) Group I mafic granulites, although their average K/Rb, Rb/Sr, K/Ba and Rb/Ba ratios (647, 0.016, 101, and 0.17) resemble the oceanic trend of MORB (OT; Shaw, 1968), the marked depletion of Rb, Ba and possible K relative to HFSE and REE is unusual. It is difficult to deduce whether this depletion is resulted from the evolution of the source magma or the loss of these elements during metamorphism. For two K- and Rb-enriched Group II mafic granulites, because their LREE abundances are very low, the enrichment of K and Rb does not reflect the protolith geochemistry, but may be caused by metamor-

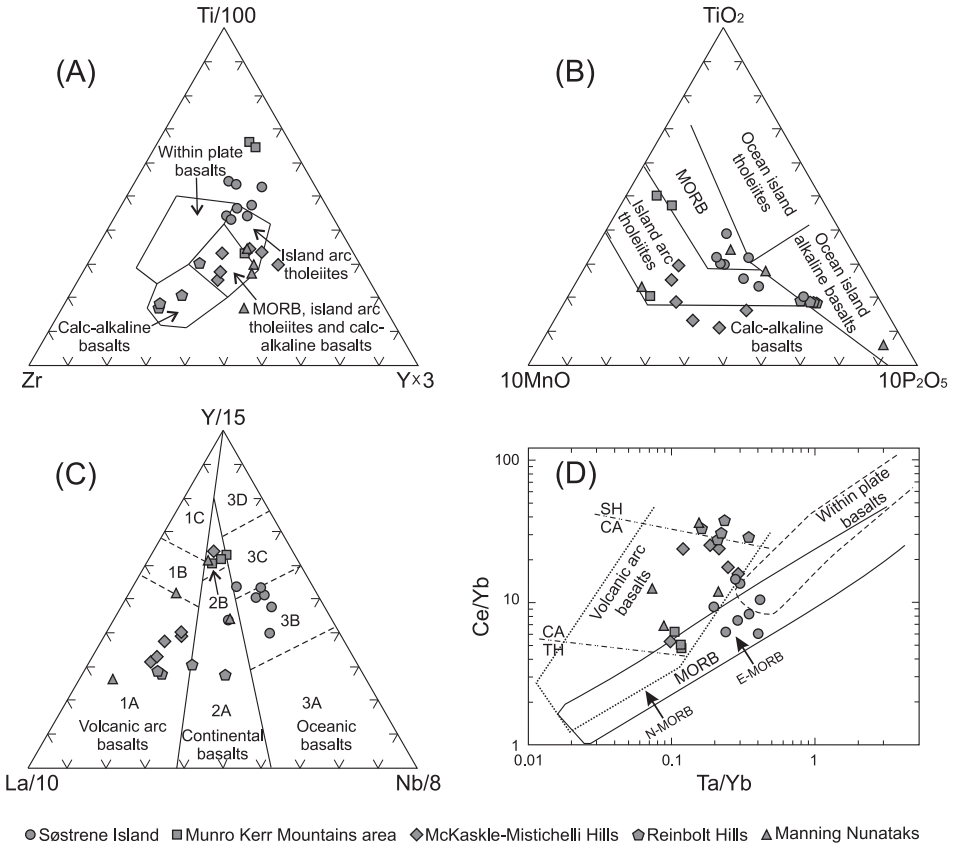

Fig. 10. Trace element discrimination diagrams for mafic granulites. (A) Zr-Ti-Y diagram (after Pearce and Cann, 1973). (B) MnO-TiO_2-P_2O_5 diagram (after Mullen, 1983). (C) La-Y-Nb diagram (after Cabanis and Lecolle, 1989). 1A—calc-alkali basalts; 1C—volcanic arc basalts; 1B—an area of overlap between 1A and 1C; 2A—continental basalts; 2B—backarc basin basalts; 3A—alkali basalts from intercontinental rift; 3B–C—E-MORB; 3D—N-MORB. (D) Ce/Yb-Ta/Yb diagram (after Pearce, 1982). SH—shoshonitic; CA—calc-alkali; TH—tholeiitic.

phic processes. In addition, different degrees of Th and U loss were also found in most mafic granulites (see fig. 9D). Consequently, the LILE cannot be used to discuss the origin and tectonic setting of protoliths of mafic granulites. The abundances and ratios of immobile REE and HFSE as well as Nd isotopic compositions are the basis for the following discussion.

Origin and Tectonic Setting of Mafic-Felsic Igneous Rocks

As mentioned previously, Group I-II mafic granulites from the Søstrene Island and Munro Kerr Mountains area exhibit REE distribution patterns and trace element spidergrams similar to E-MORB despite the unusual depletion or enrichment in some LILE. In the tectonic discrimination diagrams in terms of HFSE and REE such as Nb, Ta, Zr, Ti, P, La, Ce, Yb and Y as well as transition element Mn, most samples also fall in the E-MORB field (figs. 10A-10D), although some samples deviate towards the Ti-rich trend in the Zr-Ti-Y diagram (Pearce and Cann, 1973) and Group II samples are plotted in the field of backarc basin basalts in the La-Y-Nb diagram (Cabanis and Lecolle, 1989). The slightly evolved isotopic signatures with $\varepsilon_{Nd}(T)$ values of +4.1 to

−0.4 correspond to weakly enriched mantle source regions. In field relations, however, mafic granulites are mainly interlayered with arc-related felsic orthogneisses (see below) and minor paragneisses, or present as large lenses or blocks in them, different from the typical occurrences of remnants of oceanic crust. In fact, these mafic granulites, especially for Group I, are geochemically similar to Nb-enriched basalts, which were commonly associated with adakites in some modern and ancient island arc systems (for example, Defant and others, 1992; Kepezhinskas and others, 1996; Sajona and others, 1996; Aguillón-Robles and others, 2001; Wang and others, 2007; Sorbadere and others, 2013). With a few exceptions (for example, Castillo, 2008), most authors consider these Nb-enriched arc basalts to have originated from melting of mantle wedge peridotites, which has been metasomatized by slab-derived melts (for example, Defant and others, 1992).

Group III mafic granulites from the McKaskle-Mistichelli Hills, Reinbolt Hills and Manning Nunataks are variably enriched in LILE and significantly depleted in Nb-Ta, Zr and Ti, which are characteristic of island arc basalts. The assumption of island arc tectonic setting may be validated by trace element discrimination diagrams—almost all data points fall in the field of volcanic arc basalts/island arc tholeiites and calc-alkali basalts (see figs. 10A-10D). Therefore, these rocks are subduction-related, and the magma was derived from a mantle wedge above the subducted slab. These mafic granulites commonly have weakly negative Eu anomalies (see figs. 4C-4E), probably resulted from plagioclase fractionation during the crystallization of the protolithic magma. The $\varepsilon_{Nd}(T)$ values of these rocks mostly have a small range from −3.2 to −4.7, suggesting that the primary magma was derived from partial melting of an enriched subarc lithospheric mantle. Alternatively, participation of old crustal rocks in the magma generation is possible. In view of the similar T_{DM} ages between the mafic granulites and felsic orthogneisses, crustal contamination might have played an important role in the magma process.

Major and trace element geochemistry has indicated that felsic orthogneisses from the studied area have the characteristics of I-type or S-type granites. In the tectonic discrimination diagrams based on Rb-Y-Nb and Rb-Yb-Ta variations (Pearce and others, 1984), most samples fall in the field of volcanic arc granites (figs. 11A-11D). In general, arc-related I-type igneous rocks were generated by melting of mantle-derived or lower crustal basaltic (for intermediate compositions) and andesitic rocks (for acid compositions), or by fractional crystallization of basaltic and andesitic magma, whereas S-type granitic rocks were likely derived from partial melting of sedimentary rocks. The negative $\varepsilon_{Nd}(T)$ values of −3.1 to −7.6 for the felsic orthogneisses (excluding high Sr/Y type) indicate less importance of input of mantle-derived materials, and appear to favor a lower crustal melting for the generation of granitic magmas. The T_{DM} ages of 2.23 to 1.91 Ga suggest that the most important crustal formation in the eastern Amery Ice Shelf-southwestern Prydz Bay area took place in the Paleoproterozoic.

The high Sr/Y orthogneisses have trace element geochemical characteristics roughly similar to adakites (Defant and Drummond, 1990). Higher Sr/Y and La/Yb ratios and significant HREE depletion indicate melting of a mafic source where garnet and/or hornblende are residual phases (Martin, 1999). However, these rocks also show higher K_2O contents (3.2-5. 6 wt%) and K_2O/Na_2O ratios (1.49-2.21), pronounced positive Eu anomalies ($Eu/Eu^* = 1.47$-5.05), and negative $\varepsilon_{Nd}(T)$ values (−2.4 to −5.5), suggesting that they were not generated by partial melting of subducted oceanic crust. Such K-rich adakites have been reported from the Himalayan collisional zone of Tibet and were thought to be derived from partial melting of mafic materials in a thickened lower continental crust (for example, Chung and others, 2003; Hou and others, 2005; Wang and others, 2005; Zeng and others, 2011).

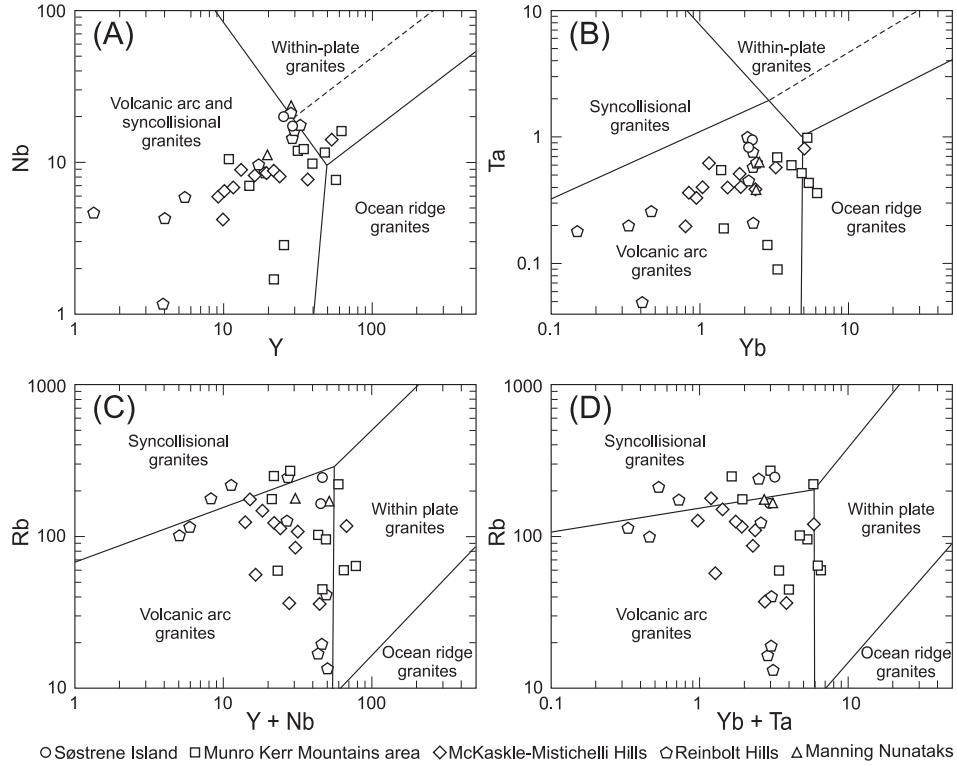

Fig. 11. Trace element discrimination diagrams for felsic orthogneisses (after Pearce and others, 1984). (A) Nb-Y diagram. (B) Ta-Yb diagram. (C) Rb-(Y + Nb) diagram. (D) Rb-(Yb + Ta) diagram.

Accordingly, we infer that the high Sr/Y orthogneisses from the studied area is probably produced by partial melting of amphibole eclogitic, garnet amphibolitic or garnet-amphibole granulitic source with a K-rich mafic bulk composition, in the deep base of the continental arc. Because of relatively lower contents of Al_2O_3 (12.7-15.2 wt%), CaO (2.0-3.8 wt%) and Sr (165-460 ppm) in the rocks, their positive Eu anomalies cannot be simply explained by accumulation of plagioclase, but reflect characteristics of the source region.

Ages of Protoliths and Metamorphism

Our new SHRIMP zircon U-Pb dating on felsic orthogneisses from the eastern Amery Ice Shelf-southwestern Prydz Bay area reveals their protolith ages: 1347 ± 22 Ma for sample 150-1, 1327 ± 29 Ma for sample 31-2, 1161 ± 6 Ma for sample 82-1, 1132 ± 43 Ma for sample 117-2, 1117 ± 37 Ma for samples 24-10, and 1079 ± 29 Ma for sample 41-1. All the age data fall in the range of 1380 to 1020 Ma (Liu and others, 2007a, 2009a; Wang and others, 2008; Grew and others, 2012) (table 6). This suggests the Mesoproterozoic magmatism in the area lasting for ~360 Ma. Although the precise ages of the late Mesoproterozoic/early Neoproterozoic metamorphism were not obtained because of the effect of variable Pb loss, two groups of age data at ~1000 to 970 and 930 to 880 Ma could be distinguished, which are similar to the results (>970 and 930-900 Ma) reported by Liu and others (2009a). In addition, the 930 to 900 Ma overgrowths on the >970 Ma zircon domains have also been observed (Liu and others, 2009a). This distinction is important because it implies two episodes (or two stages) of

TABLE 6

Summary of SHRIMP zircon U-Pb age data of metamorphic rocks from the eastern Amery Ice Shelf and southwestern Prydz Bay

Location	Sample	Rock type	Protolith Age (Ma)	Metamorphic Age (Ma)	Reference
Steinnes Peninsula	F129-1	mafic granulite		1007 ± 10	Wang and others, 2008
	9921-14	felsic orthogneiss	1133 ± 12	981 ± 13 ; 529 ± 8	Wang and others, 2008
	9926-5	felsic orthogneiss	1119 ± 13	997 ± 13 ; 546 ± 7	Wang and others, 2008
Larsenn Hills	V218-5	mafic granulite	1126 ± 20	~990-940	Wang and others, 2008
	93122-15	mafic granulite		978 ± 7	Wang and others, 2008
	K217-4	mafic granulite		~950-900	Wang and others, 2008
	K217-3	felsic orthogneiss	1126 ± 11	1031 ± 29	Wang and others, 2008
	122901	felsic orthogneiss	1124 ± 24	991 ± 12 ; 530 ± 3	Grew and others, 2012
	981227-1	paragneiss		970 ± 16	Wang and others, 2008
	S226-4	paragneiss		937 ± 21 ; 539 ± 11	Wang and others, 2008
Søstrene Island	23-34	mafic granulite		~1000-530	Liu and others, 2009a
	24-10	felsic orthogneiss	1117 ± 37	922 ± 10	This paper
Meknattane Nunataks	31-2	felsic orthogneiss	1327 ± 29	997 ± 27	This paper
	32-1	felsic orthogneiss	1208 ± 27	1051 ± 39 ; 898 ± 18	Liu and others, 2009a
Hamm Peak	38-1	felsic orthogneiss	1379 ± 13	1057 ± 25 ; 907 ± 22	Liu and others, 2009a
	41-1	felsic orthogneiss	1079 ± 29	884 ± 4	This paper
Statler Hills	82-1	felsic orthogneiss	1161 ± 6	528 ± 3	This paper
McKaskle Hills	72-1	mafic granulite	1137 ± 46		Liu and others, 2007a
	80-1	mafic granulite	1019 ± 33	533 ± 9	Liu and others, 2007a
	72-7	felsic orthogneiss	1174 ± 26	529 ± 11	Liu and others, 2007a
	71-7	paragneiss		533 ± 10	Liu and others, 2007a
Mistichelli Hills	81-7	felsic orthogneiss	1179 ± 23	968 ± 19 ; 536 ± 11	Liu and others, 2009a
Jennings Promontory	117-2	felsic orthogneiss	1132 ± 43	512 ± 3	This paper
Reinbolt Hills	142-1	mafic granulite		927 ± 29	Liu and others, 2009a
	127-1	felsic orthogneiss	1042 ± 24	925 ± 24 ; 900 ± 14	Liu and others, 2009a
Manning Nunataks	150-1	felsic orthogneiss	1347 ± 22	968 ± 97 ; 529 ± 4	This paper
	151-1	felsic orthogneiss	1056 ± 13	1042 ± 34 ; 534 ± 7	Liu and others, 2009a

high-grade metamorphism in the late Mesoproterozoic/early Neoproterozoic in the Prydz Belt. The ages of 529 ± 4, 528 ± 3 and 512 ± 3 Ma were obtained for overgrowth rims of zircon from samples 150-1, 82-1 and 117-2, respectively, which are also comparable with the youngest age group reported from the same area (Liu and others, 2007a, 2009a; Wang and others, 2008; Grew and others, 2012). This indicates that at least the major outcrops in the eastern Amery Ice Shelf-southwestern Prydz Bay area have undergone the late Neoproterozoic/Cambrian metamorphism.

Implications for Accretion-Collision Processes of the Rayner Orogen

Broadly, the geochemical and Nd isotopic characteristics of mafic granulites and felsic orthogneisses from the eastern Amery Ice Shelf and southwestern Prydz Bay can be compared with those from the northern Prince Charles Mountains (Munksgaard and others, 1992; Sheraton and others, 1996; Stephenson, 2000; Mikhalsky and others, 2001; Mikhalsky and Sheraton, 2011). The similarity further supports the suggestion that much of the basement in the Prydz Belt is an eastward extension of the Rayner Complex. Recent studies suggest that the different crustal domains of the Eastern Ghats Belt in India preserve distinct magmatic and metamorphic histories (Bose and others, 2011; Dasgupta and others, 2013, and references therein), but at least the isotopic Domain 3 (Rickers and others, 2001) resembles the Rayner Complex based on

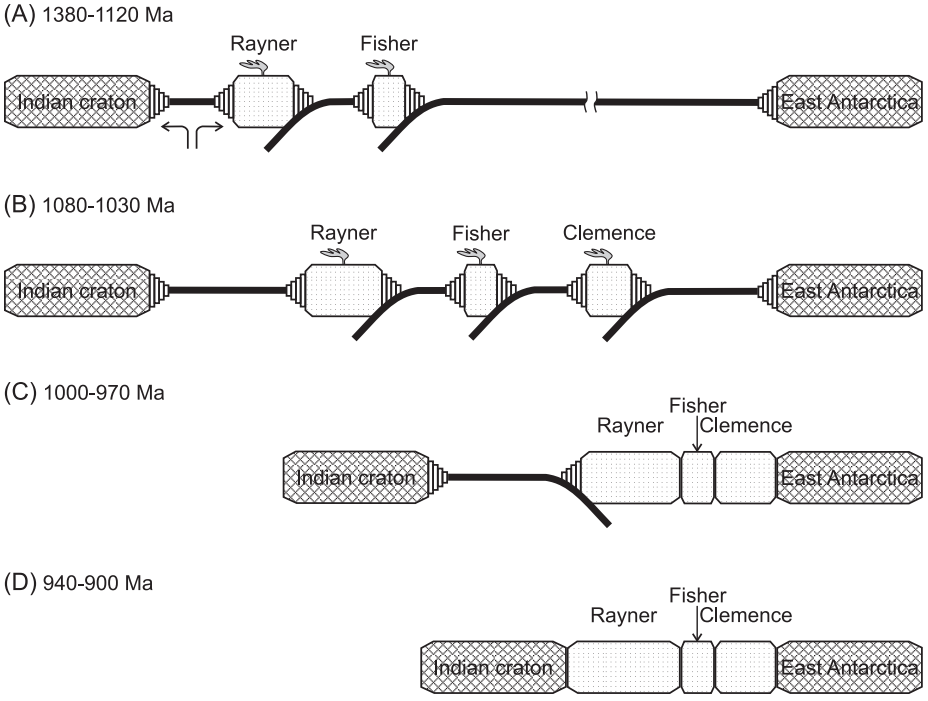

Fig. 12. Schematic cartoon showing the tectonic evolution between the Indian craton and East Antarctica (the Lambert Terrane or the Ruker craton). For explanation see text.

the similar Nd model ages (2.2-1.8 Ga). If the Rayner Complex and the Domain 3 of the Eastern Ghats Belt constitute a single continental arc, this arc would extend more than 500 km in width. As mentioned above, the SHRIMP zircon U-Pb dating in the eastern Amery Ice Shelf-southwestern Prydz Bay area indicates a prolonged period of formation of the continental arc over ~360 Ma. Regionally, the major magmatic episode of 1210 to 1120 Ma occurred in the Prydz Bay coast, McKaskle-Mistichelli Hills and their vicinity (see table 6). An older magmatic episode of 1380 to 1330 Ma was only observed in the Munro Kerr Mountains area and Luff Nunatak. By contrast, a younger episode of 1080 to 1020 Ma mainly took place in the Reinbolt Hills and Manning Nunataks, albeit this latest magmatic episode could have been more widespread in the Rayner Complex.

Rocks from the Fisher Terrane also have a calc-alkaline affinity and are inferred to have formed in island arc setting (Mikhalsky and others, 1996, 2001). In particular, some mafic rocks even show geochemical features of N-MORB and E-MORB, similar to those from the Søstrene Island and Munro Kerr Mountains area. However, both mafic and felsic igneous rocks from the Fisher Terrane have positive $\varepsilon_{Nd}(T)$ values of +3.5 to +1.6, with T_{DM} ages of 1.8 to 1.6 Ga (Mikhalsky and others, 1996, 2006). This may imply the presence of a more juvenile oceanic arc south of the Rayner continental arc during the period 1300 to 1020 Ma (fig. 12A). Such isotopically juvenile rocks have been recently reported from the Robertson Nunatak (Mikhalsky and others, 2013), suggesting that this small-scale oceanic arc extends eastward across the Lambert Graben. On the other hand, protolith ages older than 1080 Ma were not obtained from the central nunataks of the Prince Charles Mountains, including the Shaw Massif, Clemence Massif and northern end of the Mawson Escarpment (Corvino and others,

2005; Corvino and Henjes-Kunst, 2007; Maslov and others, 2007). Considering that these outcrops are located in the southeast of the Fisher Terrane and the rocks show geochemical and isotopic signatures similar to the Rayner Complex (Mikhalsky and others, 2001), we infer that a younger island arc (termed the Clemence arc) might have existed to the south of the Fisher oceanic arc (fig. 12B).

Apart from a distinct Archean complex exposed in the Rauer Group, crystalline basement older than 1400 Ma is absent in the above island arcs. Consequently, it is difficult to determine their tectonic association, that is, whether these island arcs are derived from the Indian craton (including the Napier Complex and Vestfold Block) or from the Lambert and/or Ruker Terranes. Detrital zircons from metasedimentary rocks from the Larsemann Hills and Bolingen Islands show an age population of ~1.8 to 1.6 Ga (Kelsey and others, 2008; Wang and others, 2008; Grew and others, 2012). The inherited zircon cores of ~1.6 to 1.5 Ga have also been recognized in felsic orthogneisses from the eastern Amery Ice Shelf (Liu and others, 2009a; this paper). Such ages have been frequently reported from the Domains 1A and 2 of the Eastern Ghats Belt (Bose and others, 2011; Dasgupta and others, 2013, and references therein), as well as from Kemp Land adjacent to the Napier Complex (Kelly and others, 2002; Halpin and others, 2005). However, they are almost absent in the Lambert and Ruker Terranes. Therefore, the Rayner continental arc is likely to have evolved from the Indian cratonic margin, as suggested by many authors (for example, Corvino and others, 2011; Grew and others, 2012). The development of mafic dike swarms of ~1.4 to 1.2 Ga in the Napier Complex (Sheraton and Black, 1981; Suzuki and others, 2008) and Vestfold Block (Black and others, 1991; Lanyon and others, 1993) and roughly coeval rift-related mafic to alkaline plutons (dikes) in the Domain 1A of the Eastern Ghats Belt (Upadhyay and others, 2006; Vijaya Kumar and others, 2007; Vijaya Kumar and Rathna, 2008) lends support to this conclusion. However, a recent discovery of 1.33 Ga ophiolitic mélange in the Domain 1A of the Eastern Ghats Belt (Dharma Rao and others, 2011) does not support the suggestion that the Rayner Complex was formed in an Andean-type active continental margin, but in a continental arc separated by an ocean basin from the Indian craton. Based on the geochemical data of paragneisses from the Larsemann Hills, Grew and others (2012, 2013b) suggested that the paragneiss precursors were deposited in a backarc basin located inboard of a continental arc that was active along the leading edge of the Indo-Antarctic craton. If the argument for the late Mesoproterozoic basin is correct, we would follow these authors to suggest an inner arc basin for it. This suggestion is consistent with the presence of the Eastern Ghats Belt north of the Larsemann Hills.

The formation of the Rayner orogen has been generally considered as resulting from the final collision between the Indian craton and a portion of East Antarctica (the Lambert Terrane or the Ruker craton including the Lambent Terrane). Since the ages of regional granulite facies metamorphism and syn/post-collisional charnockite and granite intrusion are bracketed between 1000 and 900 Ma, some workers proposed a protracted collision model for the Rayner orogen (Boger and others, 2000; Carson and others, 2000). However, as stated previously, the detailed SHRIMP U-Pb zircon dating may suggest two episodes (or two stages) of >970 and 930 to 900 Ma of high-grade metamorphism in the Prydz Belt. On the other hand, the granulite facies metamorphism, deformation and emplacement of syn-tectonic pegmatites in Kemp Land occurred only at 940 to 900 Ma. Coupled with the contrasting metamorphic P-T paths in Kemp Land (clockwise) and MacRobertson Land (counterclockwise), a two-stage collision model was advocated (Kelly and others, 2002; Halpin and others, 2007; Liu and others, 2013). It is inferred that several island arcs first collided with a portion of East Antarctica during 1000 to 970 Ma (fig. 12C), then followed by the closure of ocean and final collision between two continental blocks during 940 to 900 Ma (fig. 12D).

The latter tectonic process might have affected the entire Rayner orogen, leading to widespread metamorphism, deformation and pegmatite intrusion.

CONCLUSIONS

1. Mafic granulites from the Søstrene Island and Munro Kerr Mountains have the geochemical characteristics of E-type MORB, with $\varepsilon_{Nd}(T)$ values ranging from +4.1 to −0.4. They were inferred to be Nb-enriched arc basaltic rocks derived from a weakly enriched mantle wedge. By contrast, mafic granulites from the McKaskle-Mistichelli Hills, Reinbolt Hills and Manning Nunataks show typical characteristics of island arc basalts. Their $\varepsilon_{Nd}(T)$ values mostly range from −3.2 to −4.7, with T_{DM} ages of 2.3 to 1.9 Ga, suggesting their derivation from partial melting of a subarc lithospheric mantle accompanied by crustal contamination.

2. The felsic orthogneisses have the characteristics of volcanic arc granites, and one fifth of the samples belong to high Sr/Y types. They yielded $\varepsilon_{Nd}(T)$ values of −2.4 to −10.1 and T_{DM} ages of 2.2 to 1.9 Ga, implying an important episode of crustal formation in the Paleoproterozoic. The high K_2O/Na_2O ratios, positive Eu anomalies, significant HREE depletion and negative $\varepsilon_{Nd}(T)$ values for high Sr/Y orthogneisses suggest that they were not generated by partial melting of subducted oceanic crust, but by partial melting of garnet-bearing K-rich mafic sources at the lower crust of the continental arc.

3. The new SHRIMP zircon U-Pb dating on felsic orthogneisses reveals their protolith ages within the previously reported range of 1380 to 1020 Ma, and further confirms the existence of >1300 Ma arc-related rocks in the eastern Amery Ice Shelf-Prydz Bay area. These rocks subsequently experienced two episodes (or two stages) of high-grade metamorphism at >970 Ma and ~930 to 880 Ma. Furthermore, half of the dated samples record the ages of ~530 to 510 Ma, suggesting the effect of the late Neoproterozoic/Cambrian high-grade metamorphic event over much of the Prydz Belt.

4. There may exist three island arcs between the Napier Complex and Lambert Terrane in the Mesoproterozoic. The Rayner continental arc and the Fisher oceanic arc underwent a long-lived magmatic accretion for ~360 Ma. A younger island arc, that is, the Clemence arc, is inferred to have formed to the south of the Fisher arc after 1080 Ma. The tectonic evolution of the Rayner orogen may have involved an initial arc-continent collision, followed by a continent-continent collision between the Indian craton and East Antarctica (the Lambert Terrane or the Ruker craton) during the late Mesoproterozoic/early Neoproterozoic.

ACKNOWLEDGMENTS

We sincerely acknowledge Biao Song for assistance in the SHRIMP U-Pb zircon analyses. Edward Grew, Yanbin Wang and an anonymous reviewer are thanked for their critical reviews for improving the manuscript. The field work was carried out during the 2004–2005 and 2007–2008 Chinese National Antarctic Research Expedition. Logistic support by the Antarctic Administration of China and financial support by the Geological Investigation Project of China Geological Survey (1212011120176, 12120113019000), the National Natural Science Foundation of China (40872052) and the Chinese Polar Environment Comprehensive investigation & Assessment Programmes (CHINARE2012-02-05) are gratefully acknowledged. Bor-ming Jahn acknowledges the support of National Research Council (Taiwan) through grants NSC-100-2116-M-002-024 and NSC-101-2116-M-002-003.

REFERENCES

Aguillón-Robles, A., Caimus, T., Benoit, M., Maury, R. C., Cotten, J., Bourgois, J., and Michaud, F., 2001, Late Miocene adakites and Nb-enriched basalts from Vizcaino Peninsula, Mexico: Indicators of East Pacific

Rise subduction below southern Baja California: Geology, v. 29, n. 6, p. 531–534, http://dx.doi.org/10.1130/0091-7613(2001)029⟨0531:LMAANE⟩2.0.CO;2
Barbey, P., and Cuney, M., 1982, K, Rb, Sr, Ba, U and Th geochemistry of the Lapland Granulites (Fennoscandia). LILE fractionation controlling factors: Contributions to Mineralogy and Petrology, v. 81, n. 4, p. 304–316, http://dx.doi.org/10.1007/BF00371685
Beliatsky, B. V., Laiba, A. A., and Mikhalsky, E. V., 1994, U-Pb zircon age of the metavolcanic rocks of Fisher Massif (Prince Charles Mountains, East Antarctica): Antarctic Science, v. 6, n. 3, p. 355–358, http://dx.doi.org/10.1017/S0954102094000544
Black, L. P., Kinny, P. D., and Sheraton, J. W., 1991, The difficulties of dating mafic dykes: an Antarctic example: Contributions to Mineralogy and Petrology, v. 109, n. 2, p. 183–194, http://dx.doi.org/10.1007/BF00306478
Black, L. P., Kamo, S. L., Allen, C. M., Aleinikoff, J. N., Davis, D. W., Korsch, R. J., and Foudoulis, C., 2003, TEMORA 1: a new standard for Phanerozoic U-Pb geochronology: Chemical Geology, v. 200, n. 1–2, p. 155–170, http://dx.doi.org/10.1016/S0009-2541(03)00165-7
Boger, S. D., 2011, Antarctica—Before and after Gondwana: Gondwana Research, v. 19, n. 2, p. 335–371, http://dx.doi.org/10.1016/j.gr.2010.09.003
Boger, S. D., Carson, C. J., Wilson, C. J. L., and Fanning, C. M., 2000, Neoproterozoic deformation in the northern Prince Charles Mountains, East Antarctica: evidence for a single protracted orogenic event: Precambrian Research, v. 104, n. 12, p. 1–24, http://dx.doi.org/10.1016/S0301-9268(00)00079-6
Bose, S., Dunkley, D. J., Dasgupta, S., Das, K., and Arima, M., 2011, India-Antarctica-Australia-Laurentia connection in the Paleoproterozoic-Mesoproterozoic revisited: Evidence from new zircon U-Pb and monazite chemical age data from the Eastern Ghats Belt, India: Geological Society of America Bulletin, v. 123, n. 9–10, p. 2031–2049, http://dx.doi.org/10.1130/B30336.1
Cabanis, B., and Lecolle, M., 1989, Le diagramme La/10-Y/15-Nb/8: un outil pour la discrimination des séries volcaniques et la mise en évidence des processus de mélange 682 et/ou de contamination crustale: Comptes-rendus des séances de l'Académie des sciences, Série II, v. 309, p. 2023–2029.
Carson, C. J., Dirks, P. G. H. M., Hand, M., Sims, J. P., and Wilson, C. J. L., 1995, Compressional and extensional tectonics in low-medium pressure granulites from the Larsemann Hills, East Antarctica: Geological Magazine, v. 132, p. 151–170.
Carson, C. J., Fanning, C. M., and Wilson, C. J. L., 1996, Timing of the Progress Granite, Larsemann Hills: Additional evidence for Early Palaeozoic orogenesis within the East Antarctica Shield and implications for Gondwana assembly: Australian Journal of Earth Sciences, v. 43, n. 5, p. 539–553, http://dx.doi.org/10.1080/08120099608728275
Carson, C. J., Boger, S. D., Fanning, C. M., Wilson, C. J. L., and Thost, D. E., 2000, SHRIMP U-Pb geochronology from Mount Kirkby, northern Prince Charles Mountains, East Antarctica: Antarctic Science, v. 12, n. 4, p. 429–442, http://dx.doi.org/10.1017/S0954102000000523
Castillo, P. R., 2008, Origin of the adakites-high-Nb basalt association and its implications for postsubduction magmatism in Baja California, Mexico: Geological Society of America Bulletin, v. 120, n. 3–4, p. 451–462, http://dx.doi.org/10.1130/B26166.1
Chung, S. L., Liu, D. Y., Ji, J. Q., Chu, M. F., Lee, H. Y., Wen, D. J., Lo, C. H., Qian, Q., and Zhang, Q., 2003, Adakites from continental collision zones: melting of thickened lower crust beneath southern Tibet: Geology, v. 31, n. 11, p. 1021–1024, http://dx.doi.org/10.1130/G19796.1
Corvino, A. F., and Henjes-Kunst, F., 2007, A record of 2.5 and 1.1 billion year old crust in the Lawrence Hills, Antarctic Southern Prince Charles Mountains: Terra Antartica, v. 14, p. 13–30.
Corvino, A. F., Boger, S. D., Wilson, C. J. L., and Fitzsimons, I. C. W., 2005, Geology and SHRIMP U-Pb zircon chronology of the Clemence Massif, Central Prince Charles Mountains, East Antarctica: Terra Antartica, v. 12, n. 2, p. 55–68.
Corvino, A. F., Wilson, C. J. L., and Boger, S. D., 2011, The structural and tectonic evolution of a Rodinian continental fragment in the Mawson Escarpment, Prince Charles Mountains, Antarctica: Precambrian Research, v. 184, n. 1–4, p. 70–92, http://dx.doi.org/10.1016/j.precamres.2010.11.001
Dasgupta, S., Bose, S., and Das, K., 2013, Tectonic evolution of the Eastern Ghats Belt, India: Precambrian Research, v. 227, p. 247–258, http://dx.doi.org/10.1016/j.precamres.2012.04.005
Defant, M. J., and Drummond, M., S., 1990, Derivation of some modern arc magmas by melting of young subducted lithosphere: Nature, v. 347, p. 662–665, http://dx.doi.org/10.1038/347662a0
Defant, M. J., Jackson, T. E., Drummond, M., S., de Boer, J. Z., Bellon, H., Feigenson, M. D., Maury, R. C., and Stewart, R. H., 1992, The geochemistry of young volcanism throughout western Panama and southeastern Costa Rica: an overview: Journal of the Geological Society, London, v. 149, p. 569–579, http://dx.doi.org/10.1144/gsjgs.149.4.0569
Dharma Rao, C. V., Santosh, M., and Wu, Y. B., 2011, Mesoproterozoic ophiolitic mélange from the SE periphery of the Indian plate: U-Pb zircon ages and tectonic implications: Gondwana Research, v. 19, n. 2, p. 384–401, http://dx.doi.org/10.1016/j.gr.2010.06.007
Dirks, P. H. G. M., and Wilson, C. J. L., 1995, Crustal evolution of the East Antarctic mobile belt in Prydz Bay: continental collision at 500 Ma: Precambrian Research, v. 75, n. 3–4, p. 189–207, http://dx.doi.org/10.1016/0301-9268(95)80006-4
Fitzsimons, I. C. W., 1997, The Brattstrand Paragneiss and the Søstrene Orthogneiss: a review of Pan-African metamorphism and Grenvillian relics in southern Prydz Bay, *in* Ricci, C. A., editor, The Antarctic Region: Geological Evolution and Processes: Siena, Terra Antarctic Publications, p. 121–130.
——— 2003, Proterozoic basement provinces of southern and southwestern Australia, and their correlation with Antarctica, *in* Yoshida, M., Windley, B., and Dasgupta, S., editors, Proterozoic East Gondwana: Supercontinent Assembly and Breakup: Geological Society, London, Special Publication, v. 206, p. 93–130, http://dx.doi.org/10.1144/GSL.SP.2003.206.01.07
Fitzsimons, I. C. W., and Harley, S. L., 1991, Geological relationships in high-grade gneisses of the

Brattstrand Bluffs coastline, Prydz Bay, East Antarctica: Australian Journal of Earth Sciences, v. 38, n. 5, p. 497–519, http://dx.doi.org/10.1080/08120099108727987
Fitzsimons, I. C. W., Kinny, P. D., and Harley, S. L., 1997, Two stages of zircon and monazite growth in anatectic leucogneiss: SHRIMP constraints on the duration and intensity of Pan-African metamorphism in Prydz Bay, East Antarctica: Terra Nova, v. 9, n. 1, p. 47–51, http://dx.doi.org/10.1046/j.1365-3121.1997.d01-8.x
Grew, E. S., Carson, C. J., Christy, A. G., Maas, R., Yaxley, G. M., Boger, S. D., and Fanning, C. M., 2012, New constraints from U-Pb, Lu-Hf and Sm-Nd isotopic data on the timing of sedimentation and felsic magmatism in the Larsemann Hills, Prydz Bay, East Antarctica: Precambrian Research, v. 206–207, p. 87–108, http://dx.doi.org/10.1016/j.precamres.2012.02.016
Grew, E. S., Maas, R., Christy, A. G., Carson, C. J., Yates, M. G., and Boger, S. D., 2013a, A-type granites of Prydz Bay, Antarctica: Products of melting of a two-component granulite crust?: Mineralogical Magazine, v. 77, n. 5, p. 1214 (abstract).
Grew, E. S., Carson, C. J., Christy, A. G., and Boger, S. D., 2013b, Boron- and phosphate-rich rocks in the Larsemann Hills, Prydz Bay, East Antarctica: tectonic implications, *in* Harley, S. L., Fitzsimons, I. C. W., and Zhao, Y., editors, Antarctica and Supercontinent Evolution: Geological Society, London, Special Publications, v. 283, p. 73–94, http://dx.doi.org/10.1144/SP383.8
Halpin, J. A., Gerakiteys, C. L., Clarke, G. L., Belousova, E. A., and Griffin, W. L., 2005, *In-situ* U-Pb geochronology and Hf isotope analyses of the Rayner Complex, east Antarctica: Contributions to Mineralogy and Petrology, v. 148, n. 6, p. 689–706, http://dx.doi.org/10.1007/s00410-004-0627-6
Halpin, J. A., Clarke, G. L., White, R. W., and Kelsey, D. E., 2007, Contrasting *P-T-t* Paths for Neoproterozoic metamorphism in MacRobertson and Kemp Lands, East Antarctica: Journal of Metamorphic Geology, v. 25, n. 6, p. 683–701, http://dx.doi.org/10.1111/j.1525-1314.2007.00723.x
Halpin, J. A., Daczko, N. R., Milan, L. A., and Clarke, G. L., 2012, Decoding near-concordant U-Pb zircon ages spanning several hundred million years: recrystallization, metamictisation or diffusion?: Contributions to Mineralogy and Petrology, v. 163, n. 1, p. 67–85, http://dx.doi.org/10.1007/s00410-011-0659-7
Harley, S. L., 2003, Archaean-Cambrian crustal development of East Antarctica: metamorphic characteristics and tectonic implications, *in* Yoshida, M., Windley, B., and Dasgupta, S., editors, Proterozoic East Gondwana: Supercontinent Assembly and Breakup: Geological Society, London, Special Publications, v. 206, p. 203–230, http://dx.doi.org/10.1144/GSL.SP.2003.206.01.11
Heier, K. S., 1973, Geochemistry of granulite facies rocks and problems of their origin: Philosophical Transactions of the Royal Society of London, v. A273, p. 429–442, http://www.jstor.org/stable/74157
Hensen, B. J., and Zhou, B., 1995, A Pan-African granulite facies metamorphic episode in Prydz Bay, Antarctica: Evidence from Sm-Nd garnet dating: Australian Journal of Earth Sciences, v. 42, n. 3, p. 249–258, http://dx.doi.org/10.1080/08120099508728199
Hou, Z. Q., Gao, Y. F., Qu, X. M., Rui, Z. Y., and Mo, X. X., 2005, Origin of adakitic intrusives generated during mid-Miocene east-west extension in southern Tibet: Earth and Planetary Science Letters, v. 220, n. 1–2, p. 139–155, http://dx.doi.org/10.1016/S0012-821X(04)00007-X
Irvine, T. N., and Baragar, W. R. A., 1971, A guide to the chemical classification of the common volcanic rocks: Canadian Journal of Earth Sciences, v. 8, n. 5, p. 523–548, http://dx.doi.org/10.1139/e71-055
Jahn, B.-M., 1990, Origin of granulites: Geochemical constraints from Archean granulite facies rocks of the Sino-Korean craton, China, *in* Vielzeuf, D., and Vidal, Ph., editors, Granulites and Crustal Evolution: The Netherlands, Kluwer Academic Publishers, p. 471–492.
Jahn, B.-M., and Zhang, Z. Q., 1984, Archean granulite gneisses from eastern Hebei Province, China: rare earth geochemistry and tectonic implications: Contributions to Mineralogy and Petrology, v. 85, n. 3, p. 224–243, http://dx.doi.org/10.1007/BF00378102
Jahn, B.-M., Wu, F. Y., and Chen, B., 2000, Massive granitoid generation in Central Asia: Nd isotope evidence and implication for continental growth in the Phanerozoic: Episodes, v. 23, p. 82–92.
Kelly, N. M., Clarke, G. L., and Fanning, C. M., 2002, A two-stage evolution of the Neoproterozoic Rayner Structural Episode: new U-Pb sensitive high resolution ion microprobe constraints from the Oygarden Group, Kemp Land, East Antarctica: Precambrian Research, v. 116, n. 3–4, p. 307–330, http://dx.doi.org/10.1016/S0301-9268(02)00028-1
Kelsey, D. E., Wade, B. P., Collins, A. S., Hand, M., Sealing, C. R., and Netting, A., 2008, Discovery of a Neoproterozoic basin in the Prydz belt in East Antarctica and its implications for Gondwana assembly and ultrahigh temperature metamorphism: Precambrian Research, v. 161, n. 3–4, p. 355–388, http://dx.doi.org/10.1016/j.precamres.2007.09.003
Kepezhinskas, P. K., Defant, M. J., and Drummond, M., S., 1996, Progressive enrichment of island arc mantle by melt-peridotite interaction inferred from Kamchatka xenoliths: Geochimica et Cosmochimica Acta, v. 60, n. 7, p. 1217–1229, http://dx.doi.org/10.1016/0016-7037(96)00001-4
Kinny, P. D., Black, L. P., and Sheraton, J. W., 1997, Zircon U-Pb ages and geochemistry of igneous and metamorphic rocks in the northern Prince Charles Mountains, Antarctica: AGSO Journal of Australian Geology and Geophysics, v. 16, p. 637–654.
Lanyon, R., Black, L. P., and Seitz, H.-M., 1993, U-Pb zircon dating of mafic dykes and its application to the Proterozoic geological history of the Vestfold Hills, East Antarctica: Contributions to Mineralogy and Petrology, v. 115, n. 2, p. 184–203, http://dx.doi.org/10.1007/BF00321219
Liu, X. C., Jahn, B.-M., Zhao, Y., Li, M., Li, H. M., and Liu, X. H., 2006, Late Pan-African granitoids from the Grove Mountains, East Antarctica: Age, origin and tectonic implications: Precambrian Research, v. 145, n. 1–2, p. 131–154, http://dx.doi.org/10.1016/j.precamres.2005.11.017
Liu, X. C., Zhao, Y., Zhao, G. C., Jian, P., and Xu, G., 2007a, Petrology and geochronology of granulites from the McKaskle Hills, eastern Amery Ice Shelf, Antarctica, and implications for the evolution of the Prydz Belt: Journal of Petrology, v. 48, n. 8, p. 1443–1470, http://dx.doi.org/10.1093/petrology/egm024
Liu, X. C., Jahn, B.-M., Zhao, Y., Zhao, G. C., and Liu, X. H., 2007b, Geochemistry and geochronology of

high-grade rocks from the Grove Mountains, East Antarctica: Evidence for an Early Neoproterozoic basement metamorphosed during a single Late Neoproterozoic/Cambrian tectonic cycle: Precambrian Research, v. 158, n. 1–2, p. 93–118, http://dx.doi.org/10.1016/j.precamres.2007.04.005

Liu, X. C., Zhao, Y., Song, B., Liu, J., and Cui, J. J., 2009a, SHRIMP U-Pb zircon geochronology of high-grade rocks and charnockites from the eastern Amery Ice Shelf and southwestern Prydz Bay, East Antarctica: Constraints on Late Mesoproterozoic to Cambrian tectonothermal events related to supercontinent assembly: Gondwana Research, v. 16, n. 2, p. 342–361, http://dx.doi.org/10.1016/j.gr.2009.02.003

Liu, X. C., Hu, J., Zhao, Y., Lou, Y. X., Wei, C. J., and Liu, X. H., 2009b, Late Neoproterozoic/Cambrian high-pressure mafic granulites from the Grove Mountains, East Antarctica: *P-T-t* path, collisional orogeny and implications for assembly of East Gondwana: Precambrian Research, v. 174, n. 1–2, p. 181–199, http://dx.doi.org/10.1016/j.precamres.2009.07.001

Liu, X. C., Zhao, Y., and Hu, J. M., 2013, The *c.* 1000–900 Ma and *c.* 550–500 Ma tectonothermal events in the Prince Charles Mountains-Prydz Bay region, East Antarctica, and their relations to supercontinent evolution, *in* Harley, S. L., Fitzsimons, I. C. W., and Zhao, Y., editors, Antarctica and Supercontinent Evolution: Geological Society, London, Special Publications, v. 383, p. 95–112, http://dx.doi.org/10.1144/SP383.6

Martin, H., 1999, Adakitic magmas: modern analogues of Archaean granitoids: Lithos, v. 46, n. 3, p. 411–429, http://dx.doi.org/10.1016/S0024-4937(98)00076-0

Maslov, D. M., Vorobiev, D. M., and Belyatsky, B. V., 2007, Geological structure and evolution of Shaw Massif, central part of the Prince Charles Mountains (East Antarctica), *in* Cooper, A. K., Raymond, C. R., and others, editors, A Keystone in a Changing World—Online Proceedings of the 10th ISAES: USGS Open-File Report 2007-1047, Extended Abstract 124, 4 p.

Mezger, K., and Cosca, M. A., 1999, The thermal history of the Eastern Ghats Belt (India) as revealed by U–Pb and $^{40}Ar/^{39}Ar$ dating of metamorphic and magmatic minerals: implications for the SWEAT correlation: Precambrian Research, v. 94, n. 3–4, p. 251–271, http://dx.doi.org/10.1016/S0301-9268(98)00118-1

Middlemost, E. A. K., 1994, Naming materials in the magma/igneous rock system: Earth-Science Reviews, v. 37, n. 3–4, p. 215–224, http://dx.doi.org/10.1016/0012-8252(94)90029-9

Mikhalsky, E. V., and Sheraton, J. W., 2011, The Rayner Tectonic Province of East Antarctica: Compositional features and geodynamic setting: Geotectonics, v. 45, n. 6, p. 496–512, http://dx.doi.org/10.1134/S0016852111060057

Mikhalsky, E. V., Sheraton, J. W., Laiba, A. A., and Beliatsky, B. V., 1996, Geochemistry and origin of Mesoproterozoic metavolcanics rocks from Fisher Massif, Prince Charles Mountains, East Antarctica: Antarctic Science, v. 8, n. 1, p. 85–104, http://dx.doi.org/10.1017/S0954102096000120

Mikhalsky, E. V., Laiba, A. A., Beliatsky, B. V., and Stüwe, K., 1999, Geology, age and origin of the Mount Willing area (Prince Charles Mountains, East Antarctica): Antarctic Science, v. 11, n. 3, p. 338–352, http://dx.doi.org/10.1017/S0954102099000437

Mikhalsky, E. V., Sheraton, J. W., Laiba, A. A., Tingey, R. J., Thost, D. E., Kamenov, E. N., and Fedorov, L. V., 2001, Geology of the Prince Charles Mountains, Antarctica: AGSO-Geoscience Australia Bulletin, v. 247, p. 1–209.

Mikhalsky, E. V., Laiba, A. A., and Beliatsky, B. V., 2006, Tectonic subdivision of the Prince Charles Mountains: a review of geologic and isotopic data, *in* Fütterer, D. K., Damaske, D., Kleinschmidt, G., Miller, H., and Tessensohn, F., editors, Antarctica: Contributions to Global Earth Sciences: Berlin, Heidelberg, New York, Springer-Verlag, p. 69–82.

Mikhalsky, E. V., Sheraton, J. W., Kudriavtsev, I. V., Sergeev, S. A., Kovach, V. P., Kamenev, I. A., and Laiba, A. A., 2013, The Mesoproterozoic Rayner Province in the Lambert Glacier area: its age, origin, isotopic structure and implications for Australia-Antarctica correlations, *in* Harley, S. L., Fitzsimons, I. C. W., and Zhao, Y., editors, Antarctica and Supercontinent Evolution: Geological Society, London, Special Publications, v. 283, p. 35–57, http://dx.doi.org/10.1144/SP383.1

Mullen, E. D., 1983, $MnO/TiO_2/P_2O_5$: a minor element discriminant for basaltic rocks of oceanic environments and its implications for petrogenesis: Earth and Planetary Science Letters, v. 62, n. 1, p. 53–62, http://dx.doi.org/10.1016/0012-821X(83)90070-5

Munksgaard, N. C., Thost, D. E., and Hensen, B. J., 1992, Geochemistry of Proterozoic granulites from northern Prince Charles Mountains, East Antarctica: Antarctic Science, v. 4, n. 1, p. 59–69, http://dx.doi.org/10.1017/S0954102092000129

Pearce, J. A., 1982, Trace element characteristics of lavas from destructive plate boundaries, *in* Thorpe, R. S., editor, Andesites: Orogenic Andesites and Related Rocks: Chichester, Wiley, p. 525–548.

Pearce, J. A., and Cann, J. R., 1973, Tectonic setting of basic volcanic rocks determined using trace element analyses: Earth and Planetary Science Letters, v. 19, n. 2, p. 290–300, http://dx.doi.org/10.1016/0012-821X(73)90129-5

Pearce, J. A., Harris, N. B. W., and Tindle, A. G., 1984, Trace element discrimination diagrams for the tectonic interpretation of granitic rocks: Journal of Petrology, v. 25, n. 4, p. 956–983, http://dx.doi.org/10.1093/petrology/25.4.956

Rickers, K., Mezger, K., and Raith, M. M., 2001, Evolution of the continental crust in the Proterozoic Eastern Ghats Belt, India and new constraints for Rodinia reconstruction: implications from Sm-Nd, Rb-Sr and Pb-Pb isotopes: Precambrian Research, v. 112, n. 3–4, p. 183–212, http://dx.doi.org/10.1016/S0301-9268(01)00146-2

Rudnick, R. L., and Presper, T., 1990, Geochemistry of intermediate- to high-pressure granulites, *in* Vielzeuf, D., and Vidal, Ph., editors, Granulites and Crustal Evolution: The Netherlands, Kluwer Academic Publishers, p. 523–550, http://dx.doi.org/10.1007/978-94-009-2055-2_27

Rudnick, R. L., McLennan, S. M., and Taylor, S. R., 1985, Large ion lithophile elements in rocks from

high-pressure granulites facies terrains: Geochimica et Cosmochimica Acta, v. 49, n. 7, p. 1645–1655, http://dx.doi.org/10.1016/0016-7037(85)90268-6

Sajona, F. G., Maury, R. C., Bellon, H., Cotten, J., and Defant, M., 1996, High field strength element enrichment of Pliocene-Pleistocene island arc basalts, Zamboanga Peninsula, western Mindanao (Philippines): Journal of Petrology, v. 37, p. 693–726, http://dx.doi.org/10.1093/petrology/37.3.693

Shaw, D. M., 1968, A review of K-Rb fractionation trends to covariance analysis: Geochimica et Cosmochimica Acta, v. 32, n. 6, p. 573–602, http://dx.doi.org/10.1016/0016-7037(68)90050-1

Sheraton, J. W., and Black, L. P., 1981, Geochemistry and geochronology of Proterozoic tholeiite dykes of East Antarctica: evidence for mantle metasomatism: Contributions to Mineralogy and Petrology, v. 78, n. 3, p. 305–317, http://dx.doi.org/10.1007/BF00398925

——— 1983, Geochemistry of Precambrian gneisses: relevance for the evolution of the East Antarctic Shield: Lithos, v. 16, n. 4, p. 273–296, http://dx.doi.org/10.1016/0024-4937(83)90016-6

Sheraton, J. W., and Collerson, K. D., 1984, Geochemical evolution of Archaean granulite-facies gneisses in the Vestfold Block and comparisons with other Archaean gneiss complexes in the East Antarctic Shield: Contributions to Mineralogy and Petrology, v. 87, n. 1, p. 51–64, http://dx.doi.org/10.1007/BF00371402

Sheraton, J. W., Black, L. P., and McCulloch, M. T., 1984, Regional geochemical and isotopic characteristics of high-grade metamorphics of the Prydz Bay area: The extent of Proterozoic reworking of Archaean continental crust in East Antarctica: Precambrian Research, v. 26, n. 2, p. 169–198, http://dx.doi.org/10.1016/0301-9268(84)90043-3

Sheraton, J. W., Tindle, A. G., and Tingey, R. J., 1996, Geochemistry, origin, and tectonic setting of granitic rocks of the Prince Charles Mountains, Antarctica: AGSO Journal of Australian Geology and Geophysics, v. 16, p. 345–370.

Sorbadere, F., Schiano, P., Métrich, N., and Bertagnini, A., 2013, Small-scale coexistence of island-arc- and enriched-MORB-type basalts in the central Vanuatu arc: Contributions to Mineralogy and Petrology, v. 166, n. 5, p. 1305–1321, http://dx.doi.org/10.1007/s00410-013-0928-8

Stephenson, N. C. N., 2000, Geochemistry of granulite-facies granitic rocks from Battye Glacier, northern Prince Charles Mountains, East Antarctica: Australian Journal of Earth Sciences, v. 47, n. 1, p. 83–94, http://dx.doi.org/10.1046/j.1440-0952.2000.00762.x

Sun, S. S., and McDonough, W. F., 1989, Chemical and isotopic systematics of oceanic basalts: implications for mantle composition and processes, *in* Saunders, A. D., and Norry, M. J., editors, Magmatism in the Ocean Basins: Geological Society, London, Special Publications, v. 42, p. 313–345, http://dx.doi.org/10.1144/GSL.SP.1989.042.01.19

Suzuki, S., Ishizuka, H., and Kagami, H., 2008, Early to middle Proterozoic dykes in the Mt. Riiser-Larsen area of the Napier Complex, East Antarctica: tectonic implications as deduced from geochemical studies, *in* Satish-Kumar, M., Motoyoshi, Y., Osanai, Y., Hiroi, Y., and Shiraishi, K., editors, Geodynamic Evolution of East Antarctica: A Key to the East-West Gondwana Connection: Geological Society, London, Special Publications, v. 308, p. 195–210, http://dx.doi.org/10.1144/SP.308.10

Tarney, J., and Windley, B. F., 1977, Chemistry, thermal gradients and evolution of the lower continental crust: Journal of the Geological Society, London, v. 134, n. 2, p. 153–172, http://dx.doi.org/10.1144/gsjgs.134.2.0153

Thost, D. E., Hensen, B. J., and Motoyoshi, Y., 1991, Two-stage decompression in garnet-bearing mafic granulites from Søstrene Island, Prydz Bay, East Antarctica: Journal of Metamorphic Geology, v. 9, n. 3, p. 245–256, http://dx.doi.org/10.1111/j.1525-1314.1991.tb00520.x

Upadhyay, D., Raith, M. M., Mezger, K., and Hammerschmidt, K., 2006, Mesoproterozoic rift-related alkaline magmatism at Elchuru, Prakasam Alkaline Province, SE India: Lithos, v. 89, n. 3–4, p. 447–477, http://dx.doi.org/10.1016/j.lithos.2005.12.015

Vijaya Kumar, K., and Rathna, K., 2008, Geochemistry of the mafic dykes in the Prakasam Alkaline Province of Eastern Ghats Belt, India: Implications for the genesis of continental rift-zone magmatism: Lithos, v. 104, n. 1–4, p. 306–326, http://dx.doi.org/10.1016/j.lithos.2007.12.012

Vijaya Kumar, K., Frost, C. D., Frost, B. R., and Chamberlain, K. R., 2007, The Chimakurti, Errakonda, and Uppalapadu plutons, Eastern Ghats Belt, India: An unusual association of tholeiitic and alkaline magmatism: Lithos, v. 97, n. 1–2, p. 30–57, http://dx.doi.org/10.1016/j.lithos.2006.11.008

Wang, L., He, H. L., and Li, B., 2003, Multi-element determination in geological samples by Inductively Coupled Plasma Mass Spectrometry after fusion-precipitation treatment: Rock and Mineral Analysis, v. 22, p. 86–92 (in Chinese with English abstract).

Wang, Q., McDermott, F., Xu, J. F., Bellon, H., and Zhu, Y. T., 2005, Cenozoic K-rich adakitic volcanic rocks in the Hohxil area, northern Tibet: Lower-crustal melting in an intracontinental setting: Geology, v. 33, n. 6, p. 465–468, http://dx.doi.org/10.1130/G21522.1

Wang, Q., Wyman, D. A., Zhao, Z. H., Xu, J. F., Bai, Z. H., Xiong, X. L., Dai, T. M., Li, C. F., and Chu, Z. Y., 2007, Petrogenesis of Carboniferous adakites and Nb-enriched arc basalts in the Alataw area, northern Tianshan Range (western China): Implications for Phanerozoic crustal growth in the Central Asia orogenic belt: Chemical Geology, v. 236, n. 1–2, p. 42–64, http://dx.doi.org/10.1016/j.chemgeo.2006.08.013

Wang, Y., ms, 2002, Studies on the geochronology, geochemistry of the high-grade gneiss of the Larsemann Hills and its adjacent region, East Antarctica: Beijing, Chinese Academy of Geological Sciences, Ph. D. thesis, p. 1–76 (in Chinese).

Wang, Y., Liu, D., Chung, S.-L., Tong, L., and Ren, L., 2008, SHRIMP zircon age constraints from the Larsemann Hills region, Prydz Bay, for a late Mesoproterozoic to early Neoproterozoic tectono-thermal event in East Antarctica: American Journal of Science, v. 308, n. 4, p. 573–617, http://dx.doi.org/10.2475/04.2008.07

Whalen, J. B., Currie, K. L., and Chappell, B. W., 1987, A-type granites: geochemical characteristics,

discrimination and petrogenesis: Contributions to Mineralogy and Petrology, v. 95, n. 4, p. 407–419, http://dx.doi.org/10.1007/BF00402202

Williams, I. S., 1998, U-Th-Pb geochronology by ion microprobe, *in* McKibben, M. A., Shanks, W. C., III, and Ridley, W. I., editors, Applications of Microanalytical Techniques to Understanding Mineralizing Processes: Reviews in Economic Geology, v. 7, p. 1–35.

Winchester, J. A., and Floyd, P. A., 1977, Geochemical discrimination of different magma series and their differentiation products using immobile elements: Chemical Geology, v. 20, p. 325–343, http://dx.doi.org/10.1016/0009-2541(77)90057-2

Yoshida, M., 1995, Cambrian orogenic belt in East Antarctica and Sri Lanka: Implications for Gondwana assembly: A discussion: Journal of Geology, v. 103, p. 467–468, http://dx.doi.org/10.1086/629766

Young, D. N., Zhao, J.-X., Ellis, D. J., and Mcculloch, M. T., 1997, Geochemical and Sr-Nd isotopic mapping of source provinces for the Mawson charnockites, East Antarctica: implications for Proterozoic tectonics and Gondwana reconstruction: Precambrian Research, v. 86, n. 1–2, p. 1–19, http://dx.doi.org/10.1016/S0301-9268(97)00030-2

Zeng, L. S., Gao, L. E., Xie, K. J., and Zeng, J. L., 2011, Mid-Eocene high Sr/Y granites in the Northern Himalayan Gneiss Domes: Melting thickened lower continental crust: Earth and Planetary Science Letters, v. 303, n. 3–4, p. 251–266, http://dx.doi.org/10.1016/j.epsl.2011.01.005

Zhao, J.-X., Ellis, D. E., Kilpatrick, J. A., and McCulloch, M. T., 1997a, Geochemical and Sr-Nd isotopic study of charnockites and related rocks in the northern Prince Charles Mountains, East Antarctica: implications for charnockite petrogenesis and Proterozoic crustal evolution: Precambrian Research, v. 81, n. 1–2, p. 37–66, http://dx.doi.org/10.1016/S0301-9268(96)00022-8

Zhao, Y., Song, B., Wang, Y. B., Ren, L. D., Li, J. L., and Chen, T. Y., 1992, Geochronology of the late granite in the Larsemann Hills, East Antarctica, *in* Yoshida, Y., Kaminuma, K., and Shiraishi, K., editors, Recent Progress in Antarctic Earth Science: Tokyo, Terra Scientific Publishing Company, p. 155–161.

Zhao, Y., Liu, X. H., Song, B., Zhang, Z. Q., Li, J. L., Yao, Y. P., and Wang, Y. B., 1995, Constraints on the stratigraphic age of metasedimentary rocks from the Larsemann Hills, East Antarctica: possible implications for Neoproterozoic tectonics: Precambrian Research, v. 75, n. 3–4, p. 175–188, http://dx.doi.org/10.1016/0301-9268(95)80005-3

Zhao, Y., Liu, X. H., Wang, S. C., and Song, B., 1997b, Syn- and post-tectonic cooling and exhumation in the Larsemann Hills, East Antarctica: Episodes, v. 20, p. 122–127.

Zhao, Y., Liu, X. H., Liu, X. C., and Song, B., 2003, Pan-African events in Prydz Bay, East Antarctica and their implications for East Gondwana tectonics, *in* Yoshida, M., Windley, B., and Dasgupta, S., editors, Proterozoic East Gondwana: Supercontinent Assembly and Breakup: Geological Society, London, Special Publications, v. 206, p. 231–245, http://dx.doi.org/10.1144/GSL.SP.2003.206.01.12